Oncogene (2010) 29, 2181–2191

www.nature.com/onc

ORIGINAL ARTICLE

Processing of CD109 by furin and its role in the regulation of TGF-β signaling

S Hagiwara[1,2], Y Murakumo[1], S Mii[1], T Shigetomi[2], N Yamamoto[2], H Furue[2], M Ueda[2] and M Takahashi[1,3]

[1]Department of Pathology, Nagoya University Graduate School of Medicine, Nagoya, Japan; [2]Department of Oral and Maxillofacial Surgery, Nagoya University Graduate School of Medicine, Nagoya, Japan and [3]Division of Molecular Pathology, Center for Neurological Disease and Cancer, Nagoya University Graduate School of Medicine, Nagoya, Japan

CD109 is a glycosylphosphatidylinositol (GPI)-anchored glycoprotein, whose expression is upregulated in squamous cell carcinomas of the lung, esophagus, uterus and oral cavity. CD109 negatively regulates transforming growth factor (TGF)-β signaling in keratinocytes by directly modulating receptor activity. In this study, we further characterized CD109 regulation of TGF-β signaling and cell proliferation. We found that CD109 is produced as a 205 kDa glycoprotein, which is then processed in the Golgi apparatus into 180 kDa and 25 kDa proteins by furin (furinase). 180 kDa CD109 associated with GPI-anchored 25 kDa CD109 on the cell surface and was also secreted into the culture medium. To investigate whether furinase cleavage of CD109 is necessary for its biological activity, we mutated arginine 1273 in the CD109 furinase cleavage motif (amino acid 1270-RRRR-1273) to serine (R1273S). Interestingly, CD109 R1273S neither significantly impaired TGF-β signaling nor affected TGF-β-mediated suppression of cell growth, although it was expressed on the cell surface as a 205 kDa protein. Consistent with this finding, the 180 kDa and 25 kDa CD109 complex, but not CD109 R1273S, associated with the type I TGF-β receptor. These findings indicate that processing of CD109 into 180 kDa and 25 kDa proteins by furin, followed by complex formation with the type I TGF-β receptor is required for the regulation of TGF-β signaling in cancer cells and keratinocytes.
Oncogene (2010) **29,** 2181–2191; doi:10.1038/onc.2009.506; published online 25 January 2010

Keywords: CD109; furin; processing; TGF-β; cell proliferation

Introduction

A variety of growth factors are involved in the signaling pathways that regulate cancer progression or suppression. Transforming growth factor-β (TGF-β) is one of the most important growth factors for modulating the nature of cancer cells (Derynck *et al.*, 2001). TGF-β represents a large superfamily of dimeric growth factors that induce a wide range of biological responses, including cell proliferation, differentiation, migration and apoptosis. In mammals, the TGF-β superfamily can be categorized into three subfamilies: bone morphogenetic protein, activin/inhibin/nodal and TGF-β. The TGF-β subfamily is composed of three isoforms; TGF-β1, -β2 and -β3 (Dennler *et al.*, 2002). The TGF-β signaling pathway is transduced by two single transmembrane domain Ser/Thr kinase receptors; Type I (TβRI) and type II (TβRII) (Shi and Massagué, 2003). Ligand-mediated assembly of TβRI and TβRII initiates an intracellular phosphorylation cascade in which the activated TβRII transphosphorylates the GS domain of TβRI. Subsequently, TβRI phosphorylates receptor-regulated Smads (R-Smads; for example, Smad2/3), which can then bind a coSmad (for example, Smad4). R-Smad/coSmad complexes translocate and accumulate in the nucleus where they act as transcription factors of target genes (Massagué *et al.*, 2005). TGF-β/Smad signaling upregulates several inhibitors of cyclin-dependent kinases, such as $p15^{Ink4B}$, $p21^{Cip1}$ and $p27^{Kip1}$, thereby mediating G1 cell-cycle arrest and an antiproliferative effect (Moustakas *et al.*, 2002; Pardali and Moustakas, 2007). Thus, disruption of the TGF-β signaling pathway could result in enhanced cell proliferation. Indeed, mutations in TGF-β receptors or in downstream signaling molecules have been associated with the development of colorectal and pancreatic cancers (Xu *et al.*, 2000; Jakowlew, 2006).

CD109 is a glycosylphosphatidylinositol (GPI)-anchored cell surface glycoprotein and is a member of the α2-macroglobulin (α2M) -C3, C4 and C5 family (Sutherland *et al.*, 1991; Haregewoin *et al.*, 1994; Lin *et al.*, 2002). CD109 was first identified as a cell-surface antigen, detected in the lymphoid/myeloid cell line KG1a (Sutherland *et al.*, 1991). CD109 is expressed on a subset of fetal and adult $CD34^+$ bone marrow mononuclear cells, mesenchymal stem cell subsets, phytohemagglutinin-activated T lymphoblasts, thrombin-activated platelets, leukemic megakaryoblasts, endothelial cells and some human tumor cell lines (Kelton *et al.*,

Correspondence: Professor M Takahashi, Department of Pathology, Nagoya University Graduate School of Medicine, 65 Tsurumai-cho, Showa-ku, Nagoya, Aichi, 466-8550, Japan.
E-mail: mtakaha@med.nagoya-u.ac.jp
Received 4 August 2009; revised 1 December 2009; accepted 18 December 2009; published online 25 January 2010

1990; Murray *et al.*, 1999; Giesert *et al.*, 2003). Tam *et al.* (2003) and Finnson *et al.* (2006) reported that CD109 was a component of the TGF-β receptor system and that it decreased TGF-β1-induced phosphorylation of R-Smad in human keratinocytes. We recently found that CD109 was upregulated in oral squamous cell carcinoma (SCC), which resulted in a reduction of the TGF-β1-mediated anti-proliferative effect in oral SCC cells (Hagiwara *et al.*, 2008). In addition, the expression levels of the *CD109* transcript were significantly increased in SCCs of esophagus, lung and uterus (Hashimoto *et al.*, 2004; Zhang *et al.*, 2005). Immunohistochemical analyses using an anti-CD109 antibody revealed that high levels of CD109 were frequently detected in lung and oral cavity SCCs compared with other types of carcinoma (Sato *et al.*, 2007; Hagiwara *et al.*, 2008). On the other hand, CD109 immunoreactivity in normal tissues was detected in a restricted number of cell types, such as myoepithelial cells of the breast, salivary, lacrimal and bronchial secretary glands and basal cells of the prostate and bronchial epithelia (Sato *et al.*, 2007; Hagiwara *et al.*, 2008; Hasegawa *et al.*, 2007, 2008). These findings suggested that CD109 may have a critical role in cancer development, especially in SCCs.

In this study, we further analyzed CD109 regulation of TGF-β signaling. The 205 kDa glycosylated form of CD109 was processed in the Golgi apparatus into 180 kDa and 25 kDa forms by furinase. This cleavage was required for association of CD109 with TβRI, thereby negatively regulating TGF-β signaling. Our findings provide new insight into the mechanism of TGF-β signaling regulation by CD109 in cancer cells.

Results

Generation of CD109 antibodies that recognize different epitopes

Figure 1a shows the structure of the FLAG-tagged CD109 protein. It contains an amino-terminal signal sequence, a thioester signature motif (amino acids [aa.] 918–924), a potential furinase cleavage site (aa. 1270–1273) and a GPI-anchor cleavage-addition site (aa. 1420–1445) (amino acid numbering does not include the FLAG sequence). To characterize the CD109 protein, we generated three anti-CD109 antibodies; anti-CD109-2 and anti-CD109-4 are rabbit polyclonal antibodies and 11H3 is a mouse monoclonal antibody (Figure 1a, also see Materials and methods). Anti-CD109-2 and 11H3 were generated against the same peptide (aa. 1383–1399).

Western blot analyses using the lysates of HEK293 cells transfected with the FLAG-tagged CD109 cDNA revealed that anti-FLAG and anti-CD109-4 antibodies recognized a major 180 kDa and a minor 190 kDa band, whereas the anti-CD109-2 antibody recognized 190 kDa and 25 kDa bands (Figure 1b). The 11H3 monoclonal antibody also detected both 190 kDa and 25 kDa bands (Figure 1b). Anti-FLAG and anti-CD109-2 antibodies stained the plasma membrane and the cytoplasm of the HEK293–CD109 transfectants (Figure 1c). The anti-CD109-4 antibody was not available for immunocytochemistry. To confirm that these bands represent the CD109 protein, CD109 siRNA was transfected into HEK293 and HEK293–CD109 cells and also into A431 and SK-MES-1 human squamous cell carcinoma cell lines. Their lysates were then subjected to western blot analysis. The intensities of the 190 kDa, 180 kDa and 25 kDa bands were markedly reduced in CD109 siRNA-treated cells (Figure 1d), indicating that these bands represent the CD109 proteins.

CD109 is cleaved by furinase

As CD109 has a potential furinase cleavage motif (Figure 1a), we investigated whether CD109 is processed by furinase. Furin (furinase) is a major processing enzyme in the secretary pathway, and is mainly localized in the trans-Golgi network (Ouweland *et al.*, 1990; Steiner, 1998). When 293–CD109 cells were treated with a furinase inhibitor (FI-I), a novel band of 205 kDa appeared on western blots using anti-FLAG, anti-CD109-4 and anti-CD109-2 antibodies (Figure 2a). Treatment with higher concentrations of FI-I increased the intensity of the 205 kDa band. In contrast, the intensities of the 180 kDa and 25 kDa bands decreased (Figure 2a), suggesting that 205 kDa CD109 is cleaved into 180 and 25 kDa CD109 by furinase.

The minimal sequence recognized by furinase is Arg-X-(Lys/Arg)-Arg and cleavage occurs at the C-terminal peptide bond of Arg (Molloy *et al.*, 1992; Rouillé *et al.*, 1995). To confirm that CD109 is cleaved at this motif (aa. 1270–1273: -ArgArgArgArg-), the arginine at 1273 was replaced with serine (Figure 2b) and a HEK293 transfectant expressing the mutant CD109 cDNA was established (designated R1273S cells). As shown in Figure 2c, the anti-FLAG, anti CD109-2 and anti-CD109-4 antibodies all detected a major 205 kDa band and a minor 190 kDa band. The levels of 180 kDa and 25 kDa CD109 were drastically decreased in the R1273S cells. This finding further suggested that 180 and 25 kDa bands represent products processed from the 205 kDa precursor by furinase.

180 and 25 kDa forms of CD109 are localized on the plasma membrane

To elucidate which CD109 form is present on the cell surface, 293–CD109 cell surface proteins were biotinylated. 293–CD109 cell lysates were then immunoprecipitated with anti-FLAG antibody and then reacted with anti-FLAG, anti-CD109-2, anti-CD109-4 or streptavidin. As shown in Figure 3a, streptavidin detected 180 kDa and 25 kDa CD109 but not 190 kDa CD109, indicating the former two CD109 proteins are present on the cell surface. This result also indicates that 190 kDa CD109 is localized in the cytoplasm. The lysate of R1273S cells was also immunoprecipitated with anti-FLAG antibody, followed by reaction with streptavidin. This analysis showed that 205 kDa CD109 was present on the cell surface (Figure 3b).

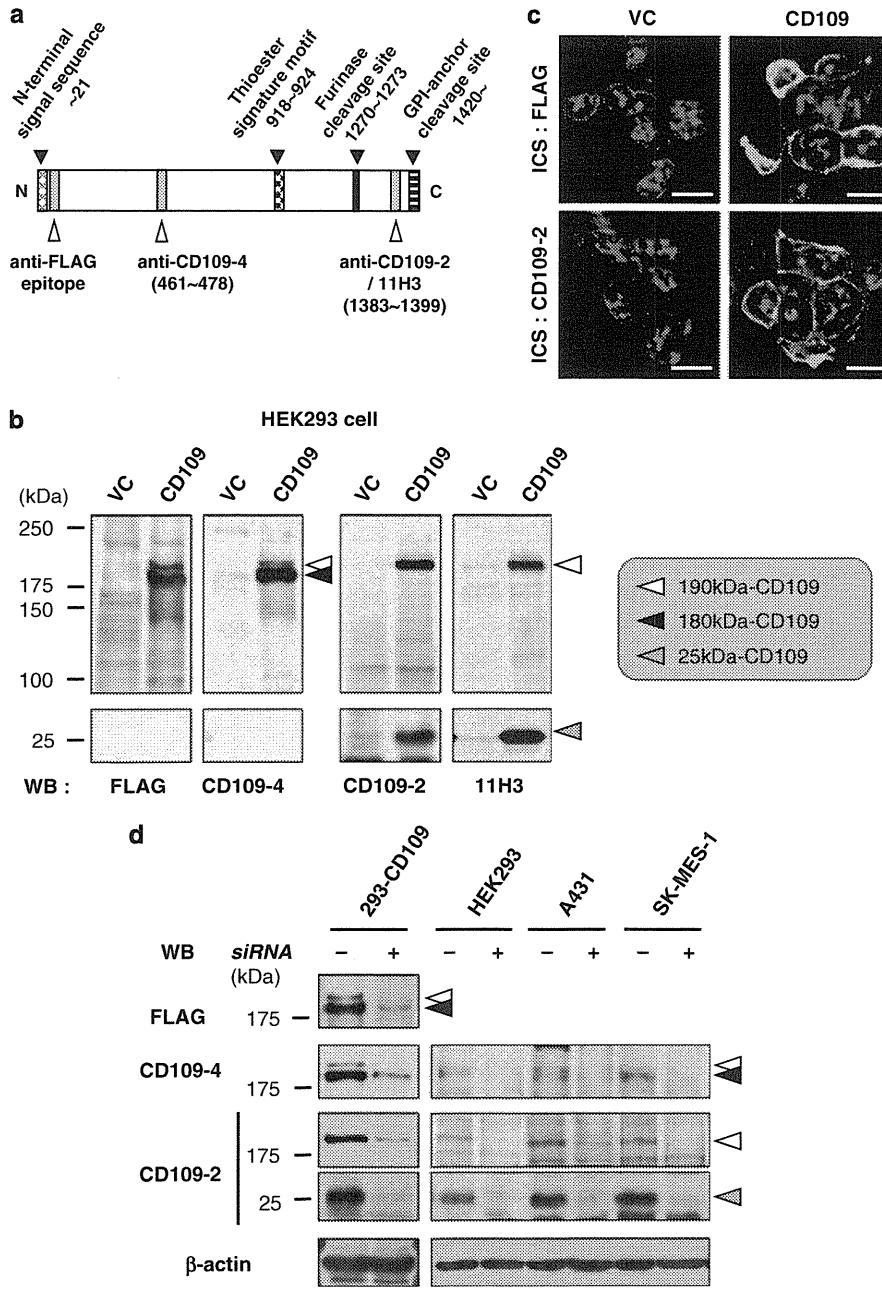

Figure 1 Expression of CD109 protein. (**a**) Schematic illustration of human CD109 protein. CD109 is a GPI-anchored glycoprotein of 1445 amino acids (aa). N-terminal signal sequence, thioester signature motif, furinase cleavage motif and C-terminal GPI-cleavage site are indicated. FLAG sequence was inserted after the N-terminal signal sequence. The peptides against which anti-CD109 polyclonal antibodies (pAb) were generated are shown (designated CD109-4 and CD109-2). 11H3 is a mouse monoclonal antibody which was generated against the same peptide as anti-CD109-2 pAb. (**b**) Detection of CD109 protein. FLAG-tagged CD109 cDNA was transfected into HEK293 cells and a stable transfectant was established. Total cell lysates were prepared from VC (vector control) and CD109-overexpressing cells, and subjected to western blot analysis with the indicated antibodies. A 190 kDa band (white arrowhead) was detected by all antibodies. 180 kDa (black arrowhead) and 25 kDa (gray arrowhead) bands were detected by anti-FLAG/CD109-4 and anti-CD109-2/11H3 antibodies, respectively. (**c**) Immunofluorescence analysis of CD109 in transfected cells. 293-VC and -CD109 transfectants were fixed and stained with anti-FLAG and anti-CD109-2 antibodies. CD109 was detected in the plasma membrane and in the cytoplasm. ICS: immunocytochemical staining. Yellow bar: 10 μm. (**d**) Knockdown of CD109 expression using siRNA. 293–CD109, HEK293, A431 (skin squamous cell carcinoma) and SK-MES-1 (lung squamous cell carcinoma) cells were treated with 50 pM CD109 siRNA and analyzed by western blotting with the indicated antibodies. Exogenous CD109 in 293–CD109 cells and endogenous CD109 in HEK293, A431 and SK-MES-1 cells were detected. Expression of 190 kDa, 180 kDa and 25 kDa CD109 was markedly decreased.

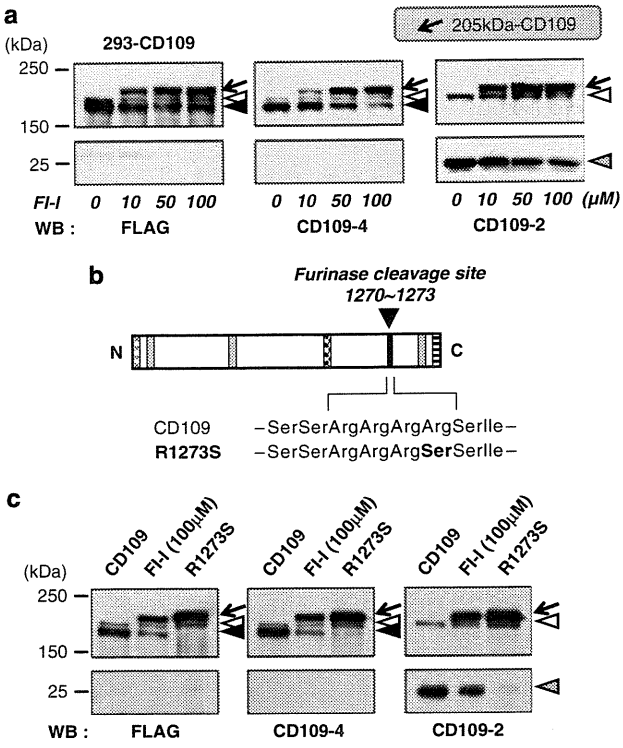

Figure 2 Cleavage of CD109 by furin. (**a**) Dose-dependent inhibition of CD109 cleavage by furinase inhibitor-I (FI-I). 293–CD109 cells were treated with the indicated concentrations of FI-I for 36 h. Total cell lysates were subjected to western blot analysis with the indicated antibodies. As the dose of FI-I increased, intensities of 180 and 25 kDa bands (black and gray arrowheads) decreased. In contrast, a novel band of 205 kDa (arrow) appeared and increased in a dose-dependant manner. (**b**) Site-directed mutagenesis of the furinase cleavage site. Arginine 1273 in CD109 was replaced with serine (designated R1273S). (**c**) Expression of CD109 R1273S. CD109 R1273S cDNA was transfected into HEK293 cells and a stable cell line (293-R1273S) was established. CD109 R1273S was expressed as a 205 kDa protein (arrow) whose molecular mass was the same as that of CD109 in FI-I-treated 293–CD109 cells. The 190 kDa band (white arrowhead) was still present in R1273S cells, but the 180 kDa and 25 kDa bands were hardly detected (black and gray arrowheads).

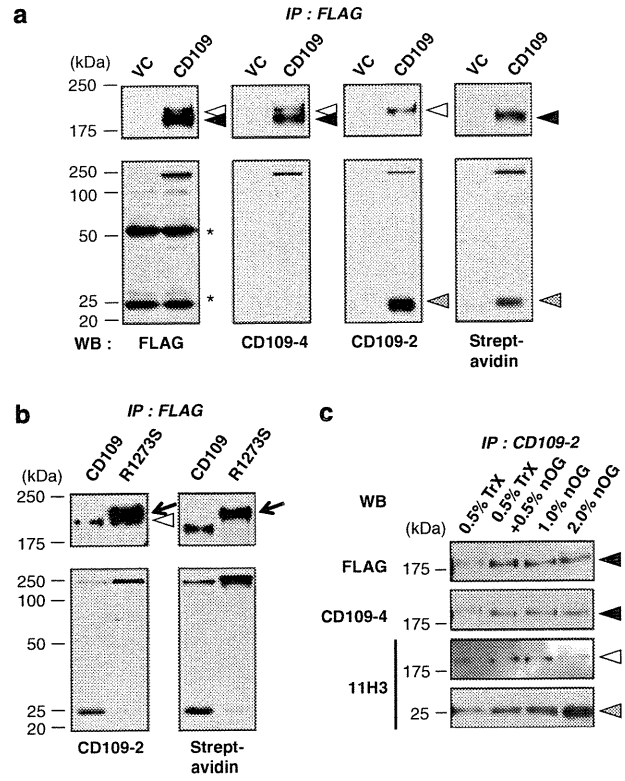

Figure 3 Subcellular localization of CD109 in transfected cells. (**a**) Cell surface localization of 180 kDa and 25 kDa CD109. Cell surface proteins of 293–CD109 cells were biotinylated and the cells were lysed with Triton X-100 buffer for immunoprecipitation (see Materials and methods). The proteins immunoprecipitated with the anti-FLAG antibody were subjected to western blot analysis with the indicated antibodies. Streptavidin detected 180 kDa and 25 kDa CD109 (black and gray arrowheads) but not 190 kDa CD109 (white arrowhead). This data indicated that 180 kDa and 25 kDa CD109 proteins were present on the cell surface, whereas 190 kDa CD109 was located in the cytoplasm. : mouse IgG heavy and light chains. (**b**) Cell surface expression of 205 kDa CD109 in R1273S cells. Cell surface proteins of 293–R1273S cells were also biotinylated and immunoprecipitated with FLAG antibody, followed by detection with streptavidin. The results showed that 205 kDa CD109 (arrow) was also localized on the cell surface. (**c**) Enrichment of 180 kDa and 25 kDa CD109 on lipid rafts. 293–CD109 cells were lysed in the absence or presence of the non-ionic detergent, *n*-Octyl-β-D-glucopyranoside (nOG), which can dissolve lipid rafts. The resultant lysate was immunoprecipitated with anti-CD109-2 antibody, followed by western blot analysis with the indicated antibodies.

GPI-anchored proteins are thought to be recruited to lipid rafts on the plasma membrane. Thus, cells were treated with the non-ionic detergent, *n*-octyl-β-D-glucopyranoside (nOG), which can dissolve lipid rafts (Garcia *et al.*, 1993). Treatment with increasing concentrations of nOG (0–2%) resulted in the immunoprecipitation of increasing amounts of 25 kDa CD109 with the anti-CD109-2 antibody (Figure 3c). In contrast, although the amount of 180 kDa CD109 detected with anti-FLAG and anti-CD109-4 antibodies increased after adding 0.5% nOG, it did not appear to increase further with higher concentrations (1–2%) of nOG. In addition, the amount of 190 kDa CD109 did not significantly change with nOG treatment (Figure 3c). These findings suggest that 25 kDa and 180 kDa CD109 is present on lipid rafts of the plasma membrane and that 25 kDa CD109 is more enriched in that fraction than 180 kDa CD109. Moreover, we found that 205 kDa R1273S mutant CD109 was enriched in the lipid raft fraction (Supplementary Figure S1).

CD109 is a glycoprotein

Based on its amino acid sequence, CD109 has 17 potential N-linked glycosylation sites. Tunicamycin completely inhibits mannose attachment on asparagine and is used for the detection of core proteins without N-linked glycosylation (Struck and Lennarz, 1977; Waechter and Harford, 1977; Guarnaccia *et al.*, 1983; Arnold *et al.*, 2006). When 293-CD109 and R1273S cells were treated with 5 μg/ml tunicamycin for 24 h, a 155 kDa

band was commonly detected using the anti-FLAG, anti-CD109-2 and anti-CD109-4 antibodies (Figure 4a). In addition, a 130 kDa band was detected with anti-FLAG and anti-CD109-4 antibodies in the lysates from tunicamycin-treated 293–CD109 cells but not from tunicamycin-treated R1273S cells. A 25 kDa CD190 band was also detected in tunicamycin-treated 293–CD109 cells (Figure 4a). We conclude from these findings that the 155 kDa protein represents a core polypeptide of CD109, without N-linked glycosylation, which is cleaved into 130 kDa and 25 kDa proteins by furinase in the Golgi apparatus of tunicamycin-treated cells. We suggest that the 155 kDa core polypeptide is processed in the endoplasmic reticulum and Golgi into the 190 kDa glycoprotein by the addition of high mannose oligosaccharides. 190 kDa CD109 is further processed into the mature glycosylated form of 205 kDa CD109, which is cleaved in the trans-Golgi network into 180 kDa and 25 kDa CD109 by furinase (Figure 4c). Finally, 180 kDa and 25 kDa CD109 are expressed on the cell surface and enriched on lipid rafts. A proposed model is illustrated in Figure 4c.

Secretion of 180 kDa CD109 into the culture medium

We next investigated whether CD109 is secreted into the culture medium. As shown in Figure 4b, 180 kDa CD109 was detected in the culture medium at a high level. Although 25 kDa CD109 and mutant 205 kDa CD109 were also detected in the medium, the ratios of 25 kDa and 205 kDa CD109 in the medium to those in the cell lysate were much lower than that of 180 kDa CD109. Thus, 180 kDa CD109 appears to be secreted into the medium as a furinase-cleaved product (Figure 4c). This finding also suggested that a small amount of 25 kDa and 205 kDa CD109 may be secreted by cleavage at the GPI-anchored site.

CD109 impairs TGF-β/Smad signaling and accelerates cell proliferation

Earlier, we showed that CD109 impaired TGF-β1-mediated suppression of cell growth using an SAS oral squamous cell carcinoma cell line (Hagiwara *et al.*, 2008). To confirm this result, we first compared the levels of Smad2 phosphorylation between 293-VC, 293-CD109 and R1273S transfectants treated with 50 pM TGF-β1 for 1 h. As shown in Figure 5a, the level of Smad2 phosphorylation in 293–CD109 cells was significantly lower than that in 293-WT (wild-type), 293-VC and R1273S cells. A cell proliferation assay revealed that 293–CD109 cells grew significantly faster than 293-VC and R1273S cells in the absence of TGF-β1. In addition, stimulation with TGF-β1 caused a significant growth suppression of 293-VC and R1273S cells, but not of 293–CD109 cells (Figure 5b), indicating that the processing of CD109 by furinase is necessary for its ability to impair the anti-proliferative effect of TGF-β1.

The time course of TGF-β/Smad signaling was further investigated for 48 h after TGF-β1 stimulation. As shown in Figure 5c, Smad2 phosphorylation and induction of p21, which is downstream of Smad signaling, were remarkably attenuated in 293–CD109 cells compared with that in 293-VC and R1273S cells. p21 is known as an inhibitor of cyclin-dependent kinase-2, and induces a suppressive effect on the cell cycle, which is consistent with the results of the cell proliferation assay shown in Figure 5b. In addition, TGF-β1 induced upregulation of endogenous CD109 expression in 293-VC cells (Figure 5c).

We next investigated whether treatment with FI-I affects TGF-β/Smad signaling in 293–CD109 cells. The levels of Smad2 phosphorylation induced by TGF-β1 did not significantly change between FI-I-untreated and treated 293–CD109 cells (Supplementary Figure S2a). This was probably because FI-I treatment did not completely inhibit the cleavage of CD109 (approximately 30% of CD109 was still processed into 180 kDa CD109 in FI-I-treated 293–CD109 cells). On the other hand, inhibition of endogenous CD109 processing in HEK293 cells moderately increased the level of Smad2 phosphorylation (Supplementary Figure S2b).

CD109 modulates receptor activity by direct interaction with TβRI, independently of ligand binding (Finnson *et al.*, 2006). We found association of 180 kDa and 25 kDa CD109 complex with TβRI by immunoprecipitation experiments, whereas the association of TβRII with CD109 appears to be very weak or non-existent. Interestingly, CD109 R1273S was not clearly associated with TβRI, indicating that the processing of CD109 into 180 kDa and 25 kDa forms is a prerequisite for association with TβRI (Figure 5d).

Overexpression of soluble 180 kDa CD109, but not C-terminal 25 kDa CD109 affects TGF-β signaling

To investigate whether 25 kDa CD109, which is GPI-anchored to lipid rafts, has an important role in TGF-β signaling, Myc-tagged C-terminal 25 kDa CD109 (designated cCD109) was constructed and cloned into pSecTag2-B (Figure 6a). cCD109 or empty vector (pSecVC) was transiently transfected into 293 cells, and after 24 h incubation, 293–cCD109 and pSecVC transfectants were subjected to western blot analysis. As shown in Figure 6b, cCD109 was detected as a 30 kDa protein using both anti-Myc and anti-CD109-2 antibodies. Cell surface expression of cCD109 was detected by immunocytochemical analysis (Figure 6c). These transfectants were stimulated with 50 pM TGF-β1 for 24 h and the levels of Smad2 phosphorylation were compared by western blot analysis (Figure 6d). Smad2 phosphorylation was observed in a similar time-dependent manner in both transfectants, although expression of exogenous cCD109 gradually decreased. This finding indicates that overexpression of 25 kDa CD109 alone does not impair TGF-β/Smad signaling.

We next generated the expression plasmid carrying a FLAG-tagged truncated CD109 (aa. 1–1273) (Figure 7a), which was transfected into HEK293 cells. As expected, this plasmid produced soluble 180 kDa CD109 proteins (designated sCD109) in the culture medium (Figure 7b). Interestingly, expression of

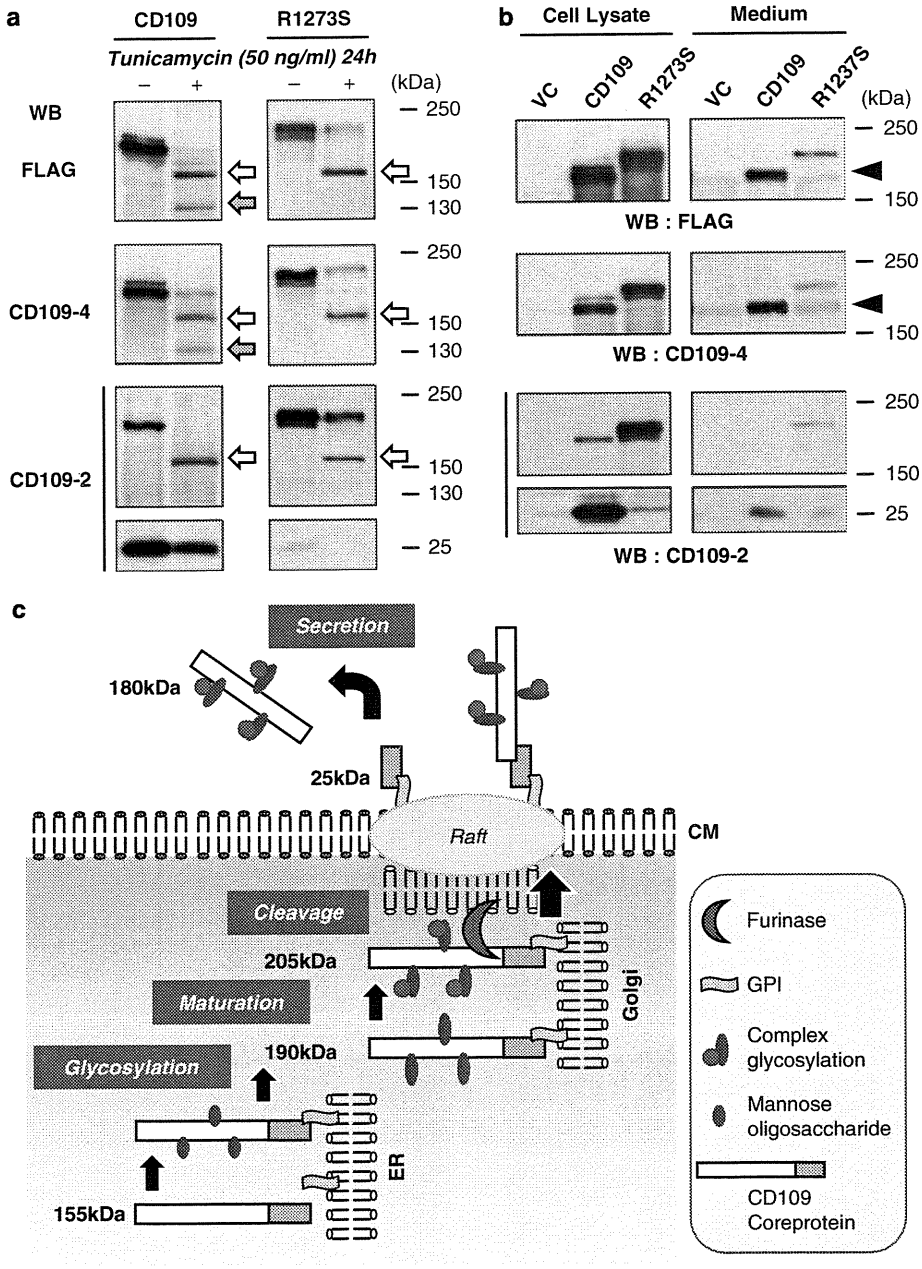

Figure 4 CD109 is a glycoprotein. (**a**) Inhibition of N-linked glycosylation by tunicamycin. 293–CD109 and R1273S cells were treated with 5 μg/ml tunicamycin for 24 h, and the resulting cell lysates were immunoblotted with the indicated antibodies. In the lysate from tunicamycin-treated cells, anti-FLAG and anti-CD109-4 antibodies detected 155 kDa (white arrow) and 130 kDa (gray arrow) bands, whereas the anti-CD109-2 antibody detected 155 kDa and 25 kDa bands. In tunicamycin-treated R1273S cells, all three antibodies detected the 155 kDa band, but hardly detected the 130 kDa and 25 kDa bands. (**b**) CD109 secretion into culture medium. Culture media from 293-VC, -CD109 and -R1273S cells, which had been incubated for 2 days, were concentrated and subjected to western blot analysis with the indicated antibodies. 180 kDa CD109 was detected at high levels in the culture medium from 293–CD109 cells by the anti-FLAG and anti-CD109-4 antibodies. 25 kDa CD109, but not 190 kDa CD109 was also detected in the medium by the anti-CD109-2 antibody, although at a low level. In addition, 205 kDa CD109 R1273S was detected at a low level in the culture medium from R1273S cells by the three antibodies. (**c**) A proposed model of CD109 protein processing. CD109 is synthesized as a 155 kDa core protein in the ER and linked to GPI. The core protein is glycosylated (high mannose type, ~190 kDa) in the ER and transferred to the Golgi complex. 190 kDa CD109 is further glycosylated (maturation, ~205 kDa) by several glycosyltransferases and then processed in the trans-Golgi network into 180 kDa and 25 kDa CD109 by furinase cleavage. Then, the complex of 180 kDa and 25 kDa CD109 is expressed on the cell surface and is enriched on lipid rafts. 180 kDa CD109 is also secreted into the culture medium.

sCD109 in HEK293 cells decreased TGF-β1-mediated Smad2 phosphorylation as observed for expression of wild-type CD109. Coexpression of cCD109 and sCD109 also decreased Smad2 phosphorylation at a similar level to that in HEK293 cells transfected with sCD109 alone (Figure 7b).

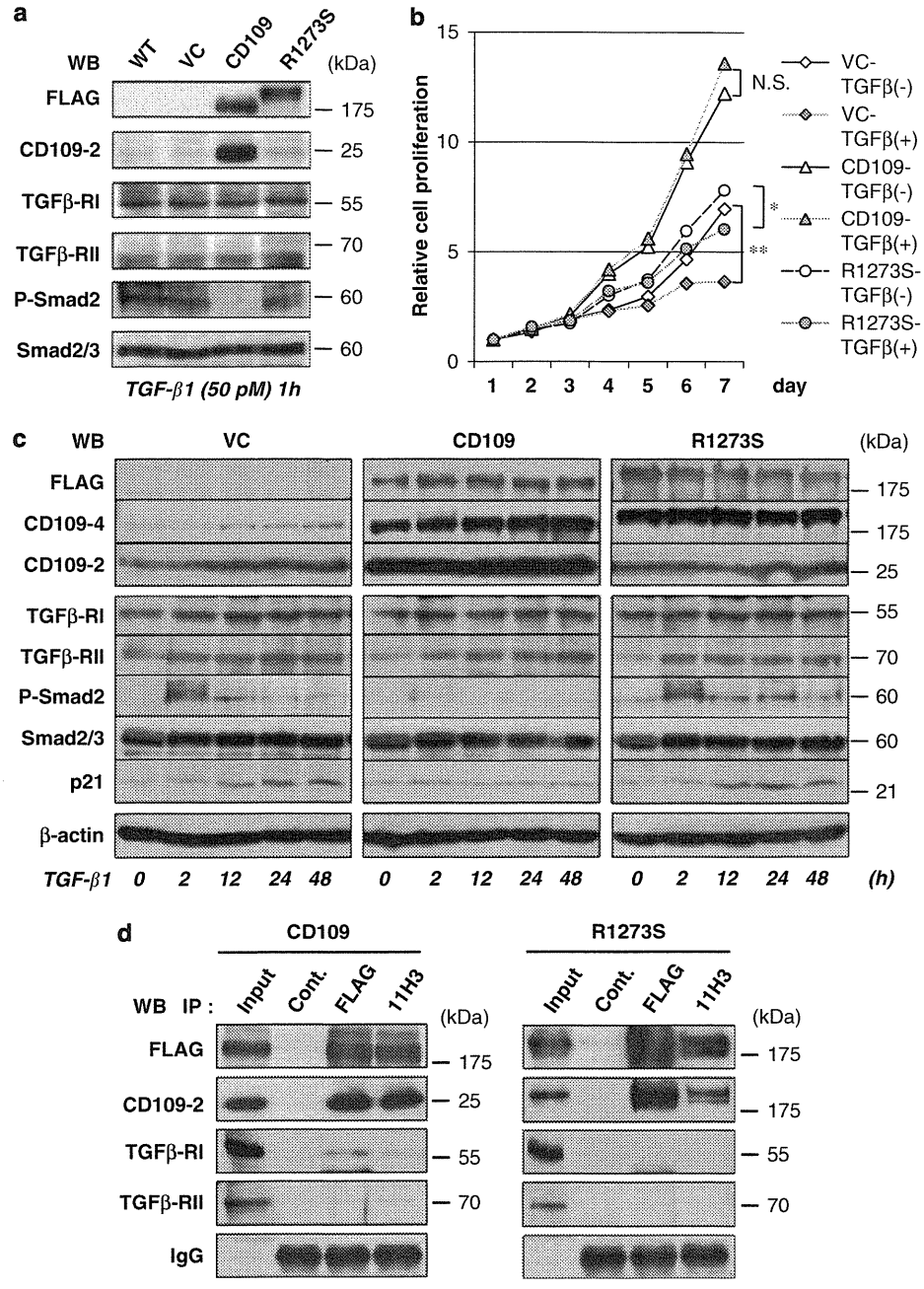

Figure 5 CD109 downregulates TGF-β/Smad signaling and accelerates cell proliferation. (**a**) CD109, but not CD109 R1273S, impairs phosphorylation of Smad2 by TGF-β1. The level of Smad2 phosphorylation (p-Smad2) in 293-WT (wild-type), 293-VC, -CD109 and -R1273S cells was assessed. The lysates from cells treated with 50 pM TGF-β1 for 1 h were subjected to western blot analysis with the indicated antibodies. The level of p-Smad in 293–CD109 cells was significantly lower than that in 293-WT, -VC, or -R1273S cells. (**b**) Cell proliferation assay in the presence or absence of TGF-β1. In the absence of TGF-β1 (TGFβ(−)), 293-CD109 cells grew significantly faster than 293-VC and R1273S cells. In the presence of 50 pM TGF-β1 (TGFβ(+)), the proliferation of 293-VC and R1273S cells was significantly suppressed after 7 days of culture, whereas the growth of 293-CD109 cells was not affected by TGF-β1 stimulation. $*P<0.05$, $**P<0.01$, NS, not significant. (**c**) Time-dependent manner of TGF-β/Smad signaling. Each transfectant was incubated with TGF-β1 for the indicated time. Smad2 phosphorylation and p21 induction by TGF-β1 in 293-CD109 cells were remarkably attenuated compared with these effects in 293-VC and -R1273S cells. (**d**) The interaction of CD109 with TGF-β receptors. The lysates from 293-CD109 or 293-R1273S cells were immunoprecipitated with normal mouse IgG (Cont.), anti-FLAG or 11H3 monoclonal antibodies, followed by western blot analysis with the indicated antibodies. CD109 but not CD109 R1273S was associated with TβRI.

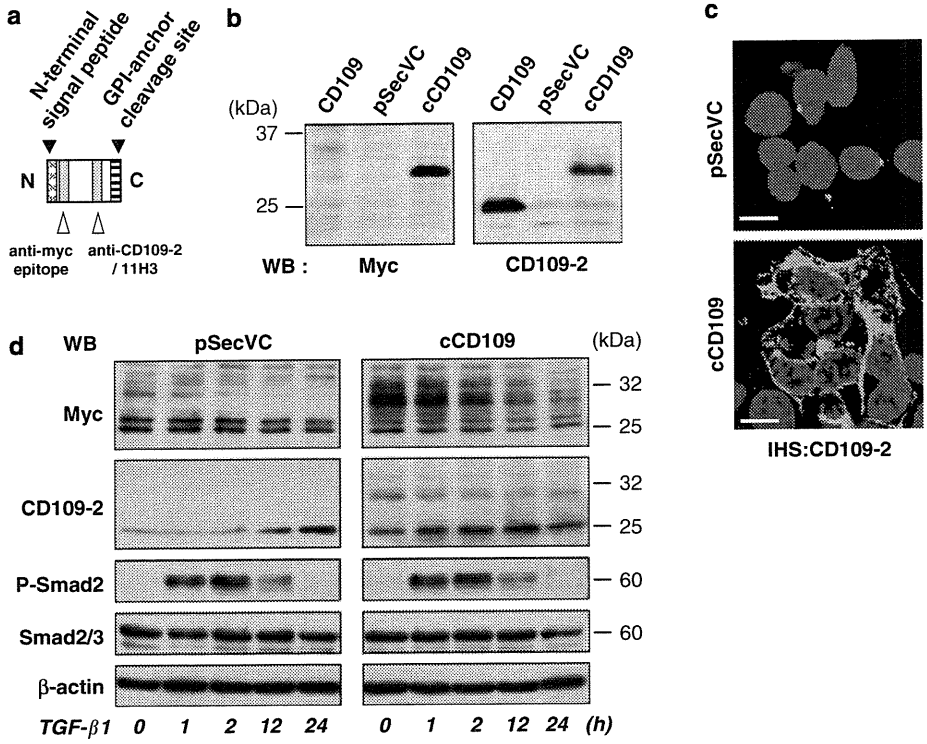

Figure 6 Expression of 25 kDa CD109 alone does not affect TGF-β/Smad signaling. (**a**) Schematic illustration of myc-tagged C-terminal CD109 (aa. 1274–1445). The construct was cloned into pSecTag2-B (designated cCD109). (**b**) Expression of cCD109 protein. CD109, cCD109 or empty vector (pSecVC) was transiently transfected in HEK293 cells, and incubated for 24 h. The lysates from 293–CD109, -cCD109 and -pSecVC cells were subjected to western blot analysis with the indicated antibodies. cCD109 was detected as a 30 kDa protein using anti-myc mAb and CD109-2 pAb. (**c**) Immunofluorescence analysis of cCD109. 24 h after transfection, 293–cCD109 and -pSecVC cells were fixed and stained with anti-CD109-2 pAb. Exogenous cCD109 was detected in the plasma membrane and in the cytoplasm. Yellow bar: 10 μm. (**d**) Time-dependent manner of TGF-β/Smad signaling. The transfectants were stimulated with 50 pM TGF-β1 for 24 h and the levels of Smad2 phosphorylation were accessed by western blot analysis at the indicated times. Both transfectants showed similar levels of Smad2 phosphorylation.

Discussion

CD109 is a GPI-anchored cell surface glycoprotein with a furinase cleavage motif. In this study, we characterized the nature and biological roles of the CD109 protein using antibodies that recognize different CD109 epitopes. We first investigated whether CD109 is cleaved by furinase. Furin is a calcium-dependent serine endoprotease that functions in the trans-Golgi network and cleaves precursor proteins into their active forms (Nakayama, 1997; Thomas, 2002). Target proteins include proparathyroid hormone, membrane type-1 matrix metalloproteinase, von Willebrand factor and TGF-β1 precursor (Gentry and Nash, 1990; Dubois *et al.*, 1995). We found that CD109 is translated as a 155 kDa core polypeptide and is processed into the 205 kDa mature glycoprotein in the Golgi via the 190 kDa immature glycoprotein (probably high mannose form). The 205 kDa CD109 was further processed by furinase into 180 kDa and 25 kDa CD109, both of which were subsequently localized on the cell surface. Treatment of CD109 transfectants with furinase inhibitor or introduction of a single amino acid substitution in the furinase cleavage motif (R1273S mutant) inhibited this processing, confirming the cleavage of CD109 by furin.

We also found that 25 kDa CD109 was a GPI-anchored protein that was highly enriched on lipid rafts. Cleaved 180 kDa CD109 was not only associated with 25 kDa CD109 but was also secreted into the culture medium. Immunoprecipitation experiments revealed the association of 25 kDa and 180 kDa CD109 complex with TβRI. These results confirmed the report by Finnson *et al.* (2006), which showed that CD109 interacted directly with TβRI, independently of ligand binding. Interestingly, the furinase-resistant CD109 R1273S was not able to associate with TβRI, although the R1273S mutant protein was localized on the cell surface. These findings indicate that processing from the 205 kDa form to the 180 kDa and 25 kDa forms by furinase cleavage is a prerequisite for the association of CD109 with TβRI on the cell surface. Further investigation is necessary to further understand the complexes that these proteins form.

CD109 R1273S lost the ability to negatively regulate TGF-β1 signaling. The levels of Smad2 phosphorylation and the expression of its downstream target, p21, were significantly decreased in wild-type CD109-expressing

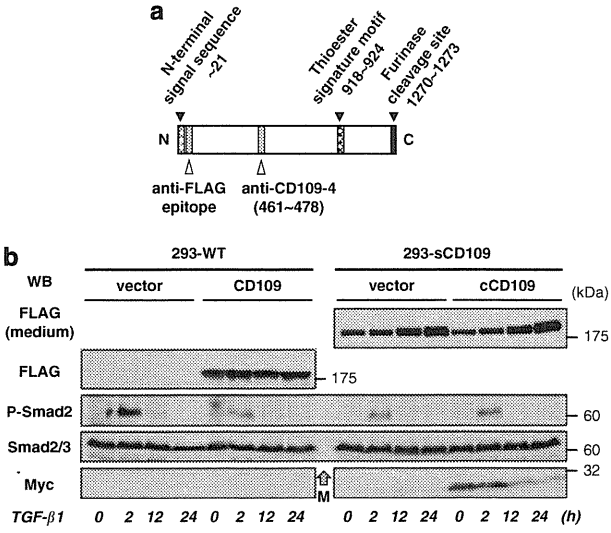

Figure 7 Expression of 180 kDa soluble CD109 impairs TGF-β/Smad signaling. (**a**) Schematic illustration of FLAG-tagged truncated CD109 (aa. 1–1273; designated sCD109). The truncated CD109 cDNA was cloned into pcDNA3.1(+). (**b**) Time-dependent manner of TGF-β/Smad signaling. A stable transfectant expressing sCD109 was established (designated 293–sCD109). 180 kDa soluble sCD109 was detected in the culture medium of the transfectant (top right panel). The transfectants expressing wild-type CD109 or sCD109 were stimulated with 50 pM TGF-β1 for 24 h and the levels of Smad2 phosphorylation were accessed by western blot analysis at the indicated times. Myc-tagged cCD109 was also transiently transfected in 293–sCD109 cells. After 24 h transfection, the cells were stimulated with 50 pM TGF-β1 for 24 h and the levels of Smad2 phosphorylation were accessed. M: marker lane.

cells, but not in CD109 R1273S-expressing cells. In addition, overexpression of CD109, but not R1273S, accelerated cell proliferation and this acceleration was not affected by TGF-β1 treatment. These results also showed that cleavage of CD109 by furinase is important for its biological functions. As overexpression of the 25 kDa form alone did not affect TGF-β1 signaling, the complex of cleaved 25 kDa and 180 kDa CD109 on the cell surface appears to regulate the function of TβRI.

We have reported that CD109 is expressed at higher levels in human SCCs of various tissues compared with other tumors of different histology. In addition, we found that in oral cancer the levels of CD109 expression were significantly higher in well-differentiated SCCs and high-risk premalignant lesions than in poorly differentiated SCCs. Furthermore, it has been reported that the levels of TβRI and TβRII expression were significantly higher in well-differentiated SCCs than in poorly differentiated SCCs (Wang *et al.*, 2009). TGF-β1 is known to have dual tumor-suppressive and promoting effects, depending on the tumor stage (Wakefield and Roberts, 2002; Bierie and Moses, 2006; Leivonen and Kähäri, 2007). TGF-β1 shows anti-proliferative effects on normal epithelial cells and during the early tumor stage. This effect then decreases and the tumor promoting effect becomes prominent as the tumor stage advances. Our findings may suggest a role of CD109 as a negative modulator of TGF-β signaling during early stages of carcinogenesis.

We show that 180 kDa CD109 is efficiently secreted into the culture medium. As CD109 binds TGF-β1 with high affinity, secreted 180 kDa CD109 may also contribute to negative regulation of TGF-β1 signaling by sequestration of TGF-β1 in the medium. However, inhibition of TGF-β signaling by CD109 can occur independently of ligand sequestration via direct modulation of TβRI activity (Finnson *et al.*, 2006). In this study, we showed that overexpression of 180 kDa soluble CD109 also inhibits TGF-β signaling, suggesting that soluble CD109 can bind to TβRI. In addition, it is worth investigating whether soluble CD109 is detected in sera from cancer patients with SCC. Establishing an assay to measure the amount of CD109 in sera may facilitate the early diagnosis of SCC or its recurrence.

Materials and methods

Cell lines

HEK293 (derived from human embryonic kidney), A431 and SK-MES-1 (derived from human skin and lung squamous cell carcinoma, respectively) cells were maintained in Dulbecco's modified Eagle's medium (DMEM) supplemented with 8% fetal bovine serum (FBS) at 37 °C in 5% CO_2. HEK293 cells expressing exogenous human CD109 were grown in 8% FBS–DMEM containing 400 μg/ml Geneticin (Invitrogen, Carlsbad, CA, USA).

Vector construction

FLAG-tagged full-length human CD109 cDNA (FLAG–CD109) was cloned into pcDNA3.1(+), as described previously (Sato *et al.*, 2007). cDNA fragments were amplified by PCR using Pfu DNA polymerase (Stratagene, La Jolla, CA, USA). The FLAG sequence, consisting of eight amino acids (aa.), was inserted just after the N-terminal signal sequence of CD109. Arginine 1273, in the furinase cleavage motif, was replaced with serine (R1273S; nucleotide 3931, A to C) by site-directed mutagenesis of FLAG-CD109. A FLAG-tagged truncated CD109 cDNA fragment (aa. 1 to 1273; designated sCD109) was also cloned into pcDNA3.1(+). A Myc-tagged C-terminal CD109 fragment (aa. 1274–1445; designated Myc-cCD109) was inserted between *Eco*RV and *Xho*I sites of pSecTag2B (Invitrogen), and transformed to *E. coli* (DH5α).

Generation of transfectants

HEK293 cells were transfected with FLAG–CD109, FLAG–$CD109^{R1273S}$ or pcDNA3.1(+) empty vector using Lipofectamine 2000 (Invitrogen). Forty eight hours after transfection, the cells were incubated for 1 week in selection medium containing 400 μg/ml of Geneticin. Geneticin-resistant colonies were picked and cultured in selection medium for another week. The expression level of CD109 in each clone was assayed by western blot analysis with anti-FLAG monoclonal antibody. Myc–cCD109 was also transfected into HEK293 cells using Lipofectamine 2000, and cells transiently expressing CD109 were prepared for several experiments.

Antibodies and reagents

Three anti-CD109 antibodies were generated by immunization with synthetic peptides of human CD109 (aa. 461–478 for

CD109-4 rabbit polyclonal antibody (pAb), aa. 1383–1399 for CD109-2 rabbit pAb and aa. 1383–1399 for 11H3; mouse monoclonal antibody (mAb)) coupled to thyroglobulin in complete Freund's adjuvant. Each antibody was affinity-purified using the immunizing peptide. Anti-FLAG M2 and β-actin mAbs were purchased from Sigma (St Louis, MO, USA). TGF-β receptor Type I, Type II and p21 pAbs were purchased from Santa Cruz Biotechnology (Santa Cruz, CA, USA). Phospho-Smad2 (Ser465/467) pAb was purchased from Cell Signaling Technologies (Beverly, MA, USA), Smad2/3 mAb was purchased from BD Biosciences (San Jose, CA, USA). Alexa-488, −594 secondary antibodies were obtained from Invitrogen, and horseradish peroxidase-conjugated anti-rabbit and anti-mouse IgG antibodies were obtained from Dako (Kyoto, Japan). Furinase Inhibitor I (FI-I; decanoyl-Arg-Val-Lys-Arg-chloromethyl ketone [dec-RVKR-cmk]), and nOG were purchased from Calbiochem (San Diego, CA, USA). Tunicamycin was purchased from Sigma. Recombinant human TGF-β1 was purchased from PeproTech (Rocky Hill, NJ, USA).

Western blot analysis
Cells were lysed with sodium dodecyl sulfate (SDS) sample buffer (62.5 mM Tris-HCl; pH 6.8, 2% SDS, 25% Glycerol, 20 μg/ml bromophenol blue), containing 1 mM phenylmethylsulfonyl fluoride and 4 mM Na_3VO_4, and sonicated until no longer viscous. After measuring the concentration of the protein using a BCA kit (Bio-Rad, Hercules, CA, USA), the lysates were boiled at 100 °C for 2 min in the presence of 2% β-mercaptoethanol. Equal amounts of protein were separated by SDS-5∼12% polyacrylamide gel electrophoresis (SDS–PAGE), and transferred to polyvinylidene difluoride membranes (Millipore, Bedford, MA, USA). Membranes were blocked for 60 min with 5% albumin in TBST buffer (20 mM Tris-HCl; pH 7.6, 137 mM NaCl, 0.1% Tween 20), and incubated with primary antibodies for 60 min at room temperature (RT). After washing the membranes three times with TBST, they were incubated with secondary antibodies for 60 min at RT. After washing the membranes, the reaction was visualized using the ECL Detection Kit (GE Healthcare, Buckinghamshire, UK).

Immunoprecipitation
Cells were lysed at 4 °C for 60 min in 500 μl of Triton X-100 buffer (1% Triton X-100, 25 mM Tris-HCl; pH 8.0, 150 mM NaCl, 10 mM EDTA, 1 mM PMSF, Complete Mini 1 Tab/10 ml) and clarified by centrifugation. The soluble fraction was pre-incubated with 10 μl of Protein A or G-Sepharose beads (Sigma) for 30 min at 4 °C. After removing the beads by centrifugation, the samples were incubated overnight at 4 °C with 0.5 μg of each precipitation antibody. The immune complexes were isolated by adding 30 μl of Protein A or G-Sepharose for 2 h at 4 °C, and these beads were washed four times with Triton X-100 buffer. The bead-bound immune complexes were resuspended in 100 μl of SDS sample buffer containing 5% β-mercaptoethanol, and heated at 100 °C for 2 min. After removing the beads by centrifugation, the samples were analyzed by SDS–PAGE.

RNA interference
SiRNA-mediated knockdown of CD109 was performed using an siGENOME SMART pool specific to human *CD109* purchased from Dharmacon (Lafayette, CO, USA). Cells were transfected with siRNA (50 nM) using Lipofectamine RNAi-MAX reagent (Invitrogen) according to the manufacturer's protocols. After incubation for 48 h, siRNA-treated cells were used for several assays.

Cell surface biotinylation
Subconfluent monolayer cells were washed three times with biotinylation buffer (10 mM HEPES; pH 8.8, 150 mM NaCl). Biotin (Long arm) NHS-Water Soluble (Vector Laboratories, Burlingame, CA, USA) was dissolved in biotinylation buffer and added to cells at a final concentration of 50 μg/ml. After incubation for 10 min at 20 °C, the reaction was terminated by the addition of NH_4Cl at a final concentration of 10 mM. Cells were washed with 50 mM Tris-HCl (pH 7.4) containing 25 mM KCl, 5 mM $MgCl_2$ and 1 mM EDTA, and lysed in Triton X-100 buffer. The lysates were used for immunoprecipitation.

CD109 processing analysis
CD109 biosynthesis and processing were analyzed using several inhibitors. A 10 mM stock solution of FI-I was prepared in DMSO and diluted into culture medium to give the required final concentration. Furin (Furinase) is a major processing enzyme, mainly localized in the trans-Golgi network, and whose minimal specific sequence is Arg-X-(Lys/Arg)-Arg (Ouweland *et al*., 1990; Molloy *et al*., 1992; Rouillé *et al*., 1995; Steiner, 1998). Tunicamycin, a streptomycete antibiotic (Takatsuki *et al*., 1971), specifically inhibits the glycosylation of proteins at asparagine residues (Struck and Lennarz, 1977; Waechter and Harford, 1977; Guarnaccia *et al*., 1983; Arnold *et al*., 2006). A 1 mg/ml tunicamycin stock solution in 10 mM NaOH was prepared, and added to culture media at a final concentration of 5 μg/ml.

Cell proliferation assay
Cells were seeded in 96-well plates (1×10^3 cells per well) in 100 μl of DMEM supplemented with 4% FBS and incubated for 24 h. After removing the medium, 100 μl of fresh medium, with or without TGF-β1, was added. The cell proliferation assay using WST-1 reagent (Roche, Basel, Switzerland) was performed according to the manufacturer's protocol. Absorbance was measured at 450–620 nm every 24 h using a microplate reader (Tecan, Palm Springs, CA, USA).

Fluorescence microscopy
Cells were fixed in 100% methanol for 20 min at −20 °C, followed by permeabilization with phosphate-buffered saline containing 0.5% Triton X-100 for 3 min. Slides were blocked in phosphate-buffered saline containing 1% BSA for 30 min at 37 °C. Samples were stained with primary antibodies for 1 h, followed by incubation with AlexaFluor 488 or 594-conjugated secondary antibody for 30 min at 37 °C. Nuclear staining was performed with DAPI or PI after incubation with secondary antibodies. The slides were mounted with PermaFluor Mounting Medium (Thermo, Pittsburgh, PA, USA). Microscopic observation was performed using an Olympus IX71/Fluoview-FV500 confocal laser scanning system at × 60 magnification.

Statistical analysis
Statistical significance of the measured values was analyzed using the two-tailed Student's *t*- test. $P<0.05$ was considered significant.

Conflict of interest

The authors declare no conflict of interest.

Acknowledgements

This work was supported by Grants-in-Aid for Global Center of Excellence (GCOE) research, Scientific Research (A) and Scientific Research on Priority Area 'Cancer' commissioned by the Ministry of Education, Culture, Sports, Science and Technology (MEXT) of Japan (to MT).

References

Arnold JN, Wallis R, Willis AC, Harvey DJ, Royle L, Dwek RA *et al.* (2006). Interaction of mannan binding lectin with α2 macroglobulin via exposed oligomannose glycans. A conversed feature of the thiol ester protein family. *J Biol Chem* **281**: 6955–6963.

Bierie B, Moses HL. (2006). Tumour microenvironment: TGFβ: the molecular Jekyll and Hyde of cancer. *Nat Rev Cancer* **6**: 506–520.

Dennler S, Goumans MJ, Ten Dijke P. (2002). Transforming growth factor beta signal transduction. *J Leukoc Biol* **71**: 731–740.

Derynck R, Akhurst RJ, Balmain A. (2001). TGF-β signaling in tumor suppression and cancer progression. *Nat Genet* **29**: 117–129.

Dubois CM, Laprise MH, Blanchette F, Gentry LE, Leduc R. (1995). Processing of transforming growth factor beta 1 precursor by human furin convertase. *J Biol Chem* **270**: 10618–10624.

Finnson KW, Tam BY, Liu K, Marcoux A, Lepage P, Roy S *et al.* (2006). Identification of CD109 as part of the TGF-β receptor system in human keratinocytes. *FASEB J* **20**: 1525–1527.

Garcia M, Mirre C, Quaroni A, Reggio H, Le Bivic A. (1993). GPI-anchored proteins associate to form microdomains during their intracellular transport in Caco-2 cells. *J Cell Sci* **104**: 1281–1290.

Gentry LE, Nash BW. (1990). The pro-domain of pre-pro-transforming growth factor beta 1 when independently expressed is a functional binding protein for the mature growth factor. *Biochemistry* **29**: 6851–6857.

Giesert C, Marxer A, Sutherland DR, Schuh AC, Kanz L, Bürring HJ. (2003). Antibody W7C5 defines a CD109 epitope expressed on CD34+ and CD34- hematopoietic and mesenchymal stem cell subsets. *Ann NY Acad Sci* **996**: 227–230.

Guarnaccia SP, Shaper JH, Schnaar RL. (1983). Tunicamycin inhibits ganglioside biosynthesis in neuronal cells. *Proc Natl Acad Sci USA* **80**: 1551–1555.

Hagiwara S, Murakumo Y, Sato T, Shigetomi T, Mitsudo K, Tohnai I *et al.* (2008). Up-regulation of CD109 expression is associated with carcinogenesis of the squamous epithelium of the oral cavity. *Cancer Sci* **99**: 1916–1923.

Haregewoin A, Solomon K, Hom RC, Soman G, Bergelson JM, Bhan AK *et al.* (1994). Cellular expression of a GPI-linked T cell activation protein. *Cell Immunol* **156**: 357–370.

Hasegawa M, Hagiwara S, Sato T, Jijiwa M, Murakumo Y, Maeda M *et al.* (2007). CD109, a new marker for myoepithelial cells of mammary, salivary, and lacrimal glands and prostate basal cells. *Pathol Int* **57**: 245–250.

Hasegawa M, Moritani S, Murakumo Y, Sato T, Hagiwara S, Suzuki C *et al.* (2008). CD109 expression in basal-like breast carcinoma. *Pathol Int* **58**: 288–294.

Hashimoto M, Ichihara M, Watanabe T, Kawai K, Koshikawa K, Yuasa N *et al.* (2004). Expression of CD109 in human cancer. *Oncogene* **23**: 3716–3120.

Jakowlew SB. (2006). Transforming growth factor-β in cancer and metastasis. *Cancer Metastasis Rev* **25**: 435–457.

Kelton JG, Smith JW, Horsewood P, Humbert JR, Hayward CP, Warkentin TE. (1990). $Gov^{a/b}$ alloantigen system on human platelets. *Blood* **75**: 2172–2176.

Leivonen SK, Kähäri VM. (2007). Transforming growth factor-β signaling in cancer invasion and metastasis. *Int J Cancer* **121**: 2119–2124.

Lin M, Sutherland DR, Horsfall W, Totty N, Yeo E, Nayar R *et al.* (2002). Cell surface antigen CD109 is a novel member of the α2 macroglobulin/C3, C4, C5 family of thioester-containing proteins. *Blood* **99**: 1683–1691.

Massagué J, Seoane J, Wotton D. (2005). Smad transcription factors. *Genes Dev* **19**: 2783–2810.

Molloy SS, Bresnahan PA, Leppla SH, Klimpel KR, Thomas G. (1992). Human furin is a calcium-dependent serine endoprotease that recognizes the sequence Arg-X-X-Arg and efficiently cleaves anthrax toxin protective antigen. *J Biol Chem* **267**: 16396–16402.

Moustakas A, Pardali K, Gaal A, Heldin CH. (2002). Mechanisms of TGF-βsignaling in regulation of cell growth and differentiation. *Immunol Lett* **82**: 85–91.

Murray LJ, Bruno E, Uchida N, Hoffman R, Nayar R, Yeo EL *et al.* (1999). CD109 is expressed on a subpopulation of CD34+ cells enriched in hematopoietic stem and progenitor cells. *Exp Hematol* **27**: 1282–1294.

Nakayama K. (1997). Furin: a mammalian subtilisin/Kex2p-like endoprotease involved in processing of a wide variety of precursor proteins. *Biochem J* **327**: 625–635.

Ouweland AM, Duijnhoven HL, Keizer GD, Dorssers LC, Ven WJ. (1990). Structural homology between the human fur gene product and the subtilisin-like protease encoded by yeast KEX2. *Nucleic Acids Res* **18**: 664.

Pardali K, Moustakas A. (2007). Actions of TGF-β as tumor suppressor and pro-metastatic factor in human cancer. *Biochim et Biophysi Acta* **1775**: 21–62.

Rouillé Y, Duguay SJ, Lund K, Furuta M, Gong Q, Lipkind G *et al.* (1995). Proteolytic processing mechanism in the biosynthesis of neuroendocrine peptides: the subtilisin-like proprotein convertases. *Front Neuroendocrinol* **16**: 322–361.

Sato T, Murakumo Y, Hagiwara S, Jijiwa M, Suzuki C, Yatabe Y *et al.* (2007). High-level expression of CD109 is frequently detected in lung squamous cell carcinomas. *Pathol Int* **57**: 719–724.

Shi Y, Massagué J. (2003). Mechanisms of TGF-beta signaling from cell membrane to the nucleus. *Cell* **113**: 685–700.

Steiner DF. (1998). The proprotein convertases. *Curr Opin Chem Biol* **2**: 31–39.

Struck DK, Lennarz WJ. (1977). Evidence for the participation of saccharide-lipids in the synthesis of the oligosaccharide chain of ovalbumin. *J Biol Chem* **252**: 1007–1013.

Sutherland DR, Yeo E, Ryan A, Mills GB, Bailey D, Baker MA. (1991). Identification of a cell-surface antigen associated with activated T lymphoblasts and activated platelets. *Blood* **77**: 84–93.

Takatsuki A, Arima K, Tamura G. (1971). Tunicamycin. a new antibiotic. I. Isolation and characterization of tunicamycin. *J Antibiot* **24**: 215–223.

Tam BY, Finnson KW, Philip A. (2003). Glycosylphosphatidylinositol-anchored proteins regulate transforming growth factor-β signaling in human keratinocytes. *J Biol Chem* **278**: 49610–49617.

Thomas G. (2002). Furin at the cutting edge: from protein traffic to embryogenesis and disease. *Nat Rev Mol Cell Biol* **3**: 753–766.

Waechter CJ, Harford JB. (1977). Evidence for the enzymatic transfer of N-acetylglucosamine from UDP-N-acetylglucosamine into dolichol derivative and glycoproteins by calf brain membranes. *Arch Biochem Biophys* **181**: 185–198.

Wakefield LM, Roberts AB. (2002). TGF-β signaling: positive and negative effects on tumorigenesis. *Curr Opin Genet Dev* **12**: 22–29.

Wang X, Sun W, Bai J, Ma L, Yu Y, Geng J *et al.* (2009). Growth inhibition induced by transforming growth factor-β1 in human oral squamous cell carcinoma. *Mol Biol Rep* **36**: 861–869.

Xu X, Brodie SG, Yang X, Im YH, Parks WT, Chen L *et al.* (2000). Haploid loss of the tumor suppressor Smad4/Dpc4 initiates gastric polyposis and cancer in mice. *Oncogene* **19**: 1868–1874.

Zhang JM, Hashimoto M, Kawai K, Murakumo Y, Sato T, Ichihara M *et al.* (2005). CD109 expression in squamous cell carcinoma of the uterine cervix. *Pathol Int* **55**: 165–169.

Supplementary Information accompanies the paper on the Oncogene website (http://www.nature.com/onc)

TISSUE ENGINEERING: Part A
Volume 16, Number 6, 2010

DOI: 10.1089/ten.tea.2009.0732

A Feasibility of Useful Cell-Based Therapy by Bone Regeneration with Deciduous Tooth Stem Cells, Dental Pulp Stem Cells, or Bone-Marrow-Derived Mesenchymal Stem Cells for Clinical Study Using Tissue Engineering Technology

Yoichi Yamada, D.D.S., Ph.D.,[1] Sayaka Nakamura, D.D.S., Ph.D.,[2] Kenji Ito, D.D.S., Ph.D.,[2]
Takayuki Sugito, D.D.S., Ph.D.,[2] Ryoko Yoshimi, D.D.S., Ph.D.,[2]
Tetsuro Nagasaka, M.D., Ph.D.,[3] and Minoru Ueda, D.D.S., Ph.D.[2]

This study investigated the effect of bone regeneration with dental pulp stem cells (DPSCs), deciduous tooth stem cells (DTSCs), or bone-marrow-derived mesenchymal stem cells (BMMSCs) for clinical study on hydroxyapatite-coated osseointegrated dental implants, using tissue engineering technology. *In vitro*, human DPSCs and DTSCs expressed STRO-1, CD13, CD29, CD 44, CD73, and osteogenic marker genes such as alkaline phosphatase, *Runx2*, and osteocalcin. *In vivo*, prepared bone defect model was implanted using graft materials as follows: platelet-rich plasma (PRP), PRP and canine BMMSCs (cBMMSCs), PRP and canine DPSCs (cDPSCs), PRP and puppy DTSCs (pDTSCs), and control (defect only). After 8 weeks, the dental implants were installed, and 16 weeks later the sections were evaluated histologically and histometrically. The cBMMSCs/PRP, cDPSCs/PRP, and pDTSCs/PRP groups had well-formed mature bone and neovascularization. Histometrically, the bone–implant contact was significantly different between the cBMMSCs/PRP, cDPSCs/PRP, pDTSCs/PRP groups, and the control and PRP groups ($p < 0.01$). These results demonstrated that these stem cells with PRP have the ability to form bone, and this bone formation activity might be useful for osseointegrated hydroxyapatite-coated dental implants with good levels of bone-implant contact.

Introduction

BONE DEFECTS AND/OR ATROPHY occurring as a result of congenital malformation, trauma, osteoporotic fractures, tumor resection, or periodontitis remain a significant health problem. Especially in an aging society, alveolar atrophy by teeth loss leads to several problems, including abnormalities of facial contours, poor fitting of dentures, mandible fragility, and mastication disorders. At present in dentistry, dental implant restoration using osseointegrated implants is regarded as a promising method, and demand is expected to increase as a consequence of increasing life expectancy and improved standards of living. This also requires special considerations, as to be successful the implant must integrate with the surrounding hard tissues before prosthetic rehabilitation. This process is defined as osseointegration and is the direct association of osseous tissue with inert alloplastic biomaterial surfaces.[1] The control of successful osseointegration around the implant during the healing period is still one of the most challenging obstacles to determine the predictability of dental implants. For rapid occlusion functional rehabilitation, a novel dental implant with a roughened surface, such as a hydroxyapatite (HA) coating, rather than implants with machine-processed titanium surfaces without coating, has been utilized.[2,3]

For dental implant placement, the presence of sufficient bone volume is an important prerequisite. Atrophic maxilla and mandible bone are less tolerant to the placement of dental implants because of their reduced height and width. These problems can be rectified by alveolar bone augmentation with autogenous bone grafting, which is considered as an ideal graft material and the gold standard. However, bone grafts require injury to the normal organization of bone in an area additional to the operation field and involve morbidity.[4]

[1]Center for Genetic and Regenerative Medicine, Nagoya University School of Medicine, Nagoya, Aichi, Japan.
[2]Department of Oral and Maxillofacial Surgery and [3]Laboratory Medicine, Nagoya University Graduate School of Medicine, Nagoya, Aichi, Japan.

On the other hand, a previous approach to this problem focused on the development of various graft materials, and bone allografts, xenografts, and alloplasts (substitutes) are being studied extensively to avoid the harvesting procedure of autogenous bone.[5] Bone substitutes, such as HA, β-tricalcium phosphate ceramics, or coral scaffolds,[6] suffer from increased susceptibility to infection, incidences of extrusion, and an uncertain long-term interaction with the host's physiology. Therefore, the present study tried to regenerate bone with minimal invasiveness by tissue engineering using stem cells for dental implants.

Recently, bone tissue engineering has been most commonly represented by the concept of an implantable construct made up of a scaffold/matrix in combination with stem/progenitor cells and/or growth factors. Tissue-engineered constructs, *ex vivo* cell propagation, and cell encapsulation all require some type of interaction between cells and the supporting material for growth, function, and/or delivery,[7,8] and stem cells are in contact with such biomaterials (as scaffolds or matrices). Generally, it is desirable for bone grafts or biomaterials for bone regeneration to be capable of osteoinduction, in which the matrix contains growth factors and/or provide a source of mature or progenitor bone cells.

Until now, bone-marrow-derived mesenchymal stem cells (BMMSCs) as the isolated cells, and platelet-rich plasma (PRP) as the growth factor source and scaffold have been explored in clinical trials for the effective treatment of osseous defects, and favorable results have been obtained.[9–13] The PRP is a mixture of growth factors, such as platelet-derived growth factors, transforming growth factor-β, as well as insulin-like growth factor-I and an autologous modification of the fibrin glue.[14] PRP stimulates the migration, proliferation, and differentiation of osteoprogenitor cells or osteoblasts. On the other hand, BMMSCs are good candidates for the treatment of mesenchymal tissue disorders, and their potential use in the setting of autologous or allogeneic hematopoietic stem cell transplantation, organ transplant rejection, and treatment of autoimmune disorders is envisaged. Recently, the engraftment of allogeneic bone-marrow-derived mesenchymal cells and growth stimulation has been demonstrated in children with imperfect osteogenesis.[15] Although BMMSCs are very useful for clinical applications, bone marrow aspiration for MSCs extraction is an invasive and painful procedure for the donor. In addition, the number, proliferation, and differentiation potential of BMMSCs declines with increasing age.[16] Another promising source for stem cells is from dental pulp, a loose vascular connective tissue surrounded by dentine and consisting of a heterogeneous population of cells. Moreover, it has been demonstrated that multipotent MSCs from dental pulp display increased immunosuppressive activity when compared with bone marrow mesenchymal cells.[17] Therefore, these cells seem to have immunosuppressive activity that could have potential clinical applications in allogenic *in vivo* stem cell transplantation, particularly for calcified tissue reconstruction.[17]

Previous studies have indicated that oral and maxillofacial bone and dental tissues contain a variety of stem cells, such as dental pulp stem cells (DPSCs), stem cells from human exfoliated deciduous teeth (SHED), and MSCs.[18,19] DPSCs and SHED possess higher proliferation capacities than BMMSCs[18,20,21] and have also have been identified as a novel population of stem cells that have the capacity of self-renewal and multilineage differentiation.[19,20,22] The main advantage of using SHED is that these can be obtained noninvasively from deciduous teeth that are routinely extracted in childhood and generally discarded as medical waste without any ethics concerns. SHED might be also capable of generating high amounts of bone *in vivo*.

An important aim of tissue engineering and regenerative medicine (TERM) is to restore tissue function using implants. However, it remains unclear whether cells used in bone regeneration applications produce a material that mimics the structure and compositional complexity of native bone. At present, no experimental studies have examined the potential of alloplastic stem-cell-based tissue-engineered bone regeneration or the correlation with osseointegrated dental implants for use in occlusion restoration. Therefore, the present study explored the bone regeneration ability of various stem cells, autologous BMMSCs, DPSCs, and allogous deciduous tooth stem cells (DTSCs), *in vitro* and whether they are able to function in dental implants even with allografts of the stem cells *in vivo*. Successful osseointegration in HA-coated dental implants on tissue-engineered bone regeneration could be obtained using a combination of BMMSCs, DPSCs, or DTSCs and PRP with minimal invasiveness.

Materials and Methods

Subjects, cell cultures, and immunofluorescence for STRO-1

Human dental pulp tissues were obtained from extracted deciduous teeth and permanent teeth. The ethics committee of Nagoya University approved the experimental protocols (permission number 548). Human DPSCs (hDPSCs) and human DTSCs (hDTSCs) were isolated and cultured as described previously.[19,21] Human BMMSCs (hBMMSCs) were purchased from Lonza® (Walkersville, MD) and cultured in accordance with the manufacturer's instructions. Canine BMMSCs (cBMMSCs), DPSCs (cDPSCs), and puppy DTSCs (pDTSCs) also were isolated and culture by the same method. Briefly, cBMMSCs were isolated from adult dogs' iliac crest marrow aspirate (10 mL), dental pulp tissues were extracted from deciduous teeth of puppies and the permanent teeth of their parents, and cBMMSCs, cDPSCs, and pDTSCs were isolated and cultured. The basal medium, low-glucose Dulbecco's modified Eagle's medium, and growth supplements (50 mL mesenchymal cell growth supplement, 10 mL of 200 mM L-glutamine, and 0.5 mL penicillin–streptomycin mixture containing 25 units penicillin and 25 μg streptomycin) were purchased from Lonza. Three supplements for inducing osteogenesis, dexamethasone, sodium β-glycerophosphate, and L-ascorbic acid 2-phosphate, were purchased from Lonza. The cells were incubated at 37°C in a humidified atmosphere containing 95% air and 5% CO_2. In culture, cMSCs, cDPSCs, and pDTSCs were trypsinized and used for implanting.

For immunofluorescence analysis of STRO-1 in hDPSCs and hDTSCs, the cells were fixed in 3% paraformaldehyde, rinsed twice with phosphate-buffered saline, and treated with 100 mM glycine for 20 min. The cells were then permeabilized with 0.2% Triton-X for 30 min and subsequently

incubated in a mixture of 5% donkey serum and 0.5% bovine serum albumin for 20 min. Next, the cells were incubated with primary mouse anti-human STRO-1 antibody (1:100; R&D, Minneapolis, MN) for 1 h, incubated for 30 min with a secondary goat anti-mouse IgM-FITC antibody (1:500; Southern Biotech, Birmingham, AL), and mounted using Vectashield with DAPI (Vector Laboratories, Burlingame, CA). The cells were examined under a fluorescence microscope (Microscope BX51; Olympus, Tokyo, Japan).

Flow cytometry analysis

Cultured cells were trypsinized, centrifuged, and washed with phosphate-buffered saline. Cells were incubated for 45 min at 4°C with specific antibodies. Fluorescein-isothiocyanate-conjugated mouse antibodies against human CD14 (BD Pharmingen, San Diego, CA), phycoerythrin-conjugated mouse antibodies against human CD73 (BD Pharmingen), allophycocyanin-conjugated mouse antibodies against human CD13, CD29, and CD34 (BD Pharmingen), and biotin-conjugated mouse antibody against human CD44 (BD Pharmingen) were used to analyze specific surface antigens. PerCP-conjugated streptavidin (BD Pharmingen) was used as the secondary antibody to detect biotin-conjugated mouse antibody against human CD44. Cell fluorescence was evaluated by flow cytometry using FACS Calibur (BD Pharmingen).

Real-time reverse transcription polymerase chain reaction analysis

On days 7, 14, 21, and 28 of cultivation in the osteoinduction medium, cells were lysed to extract total RNA using an RNeasy Mini Kit (Qiagen, Valencia, CA). A real-time reverse transcription–polymerase chain reaction (RT-PCR) analysis was conducted according to the reported method.[23,24] Specific primers and probes for the real-time RT-PCR analysis of the alkaline phosphatase (*ALP*), *Runx2*, and osteocalcin (*OCN*) gene mRNAs are shown in Table 1. The glyceraldehyde 3-phophate dehydrogenase (*GAPDH*) primer and probe (TaqMan GAPDH detection reagents) were purchased from Perkin-Elmer and Applied Biosystems (Foster City, CA), respectively. The conditions for PCR were as follows: 1 cycle at 50°C for 2 min; 1 cycle at 60°C for 30 min; 1 cycle at 95°C for 5 min; and 50 cycles at 95°C for 20 s and 60°C for 1 min. The relative amounts of the respective mRNAs in different samples were compared through factors that had been obtained by dividing the relative amount of each mRNA with that of the GAPDH mRNA in each sample; the relative amounts were designated as expression coefficients in the present study.

Canine animal models

All animal experiments undertaken in this study were performed in strict accordance with protocols approved by the Institutional Animal Care Committee. After a period of housing, adult hybrid dogs with a mean age of 2 years were operated on under general anesthesia. The first molar, premolars, and the second and third premolars in the mandible region were extracted and the healing period was 2 months. Bone defects on both sides of the mandible were prepared using a trephine bar with a diameter of 10 mm. The defects were implanted with graft materials as follows: PRP, PRP plus cBMMSCs, PRP plus cDPSCs, PRP plus pDTSCs, and control (defect only). With no differences in bone regeneration in the various grafted areas in terms of bone healing, three defects were created and implanted with four materials at random sites. After 8 weeks, an HA-coated osseointegrated dental implant was inserted into the bone regeneration areas (Fig. 3).

Injection of PRP, cBMMSCs/PRP, cDPSCs/PRP, and pDTSCs/PRP admixtures

PRP and the relevant conditions were prepared as described previously.[11] Bovine thrombin in powder form (5000 units) was dissolved in 5 mL of 10% calcium chloride. Next, 3.5 mL of PRP (1.0×10^7 cells/mL) and air were aspirated into a syringe; in another syringe, 500 μL of thrombin/calcium chloride mixture was aspirated. The two syringes were connected with a T-connector and the plungers of the syringes were pushed and pulled alternatively. Within 5–30 s, the contents assumed a gel-like consistency as the thrombin affected the polymerization of fibrin to produce an insoluble gel. The gel was injected into the bone defect field.

HA-coated dental implant insertion, and histological and histomorphometric analysis

Each implantation site was excised with a trephine bar with a diameter of 2 mm at 8 weeks after implantation and was assessed histologically. The specimens were fixed in 10% buffered formalin, decalcified (K-CX; Falma, Tokyo, Japan), and stained with hematoxylin and eosin. Then, Φ3.7 × 7 mm HA-coated JMM implants (POI/Finatite, Japan Medical

TABLE 1. PRIMER AND PROBE SEQUENCES USED IN REAL-TIME RT-PCR

Gene	*GenBank no.*		*Primer and probe sequences*
ALP	NM_000478	Forward primer	AGAAAGCCAGGGGCACGAG
		Reverse primer	GGGAGTGCTTGTATCTCGGTTTG
		Probe	CCTGGACCTCGTTGACACCTGGAAGAGC
Runx2	NM_004348	Forward primer	GCATGTCCCTCGGTATGTCC
		Reverse primer	GGTCCACTCTGGCTTTGGG
		Probe	ACCACTCACTACCACACCTACCTGCCAC
OCN	NM_000711	Forward primer	AGAGTCCAGCAAAGGTGCAG
		Reverse primer	CCCAGCCATTGATACAGGTAGC
		Probe	CTTCACTACCTCGCTGCCCTCCTGCT

RT-PCR, reverse transcription polymerase chain reaction.

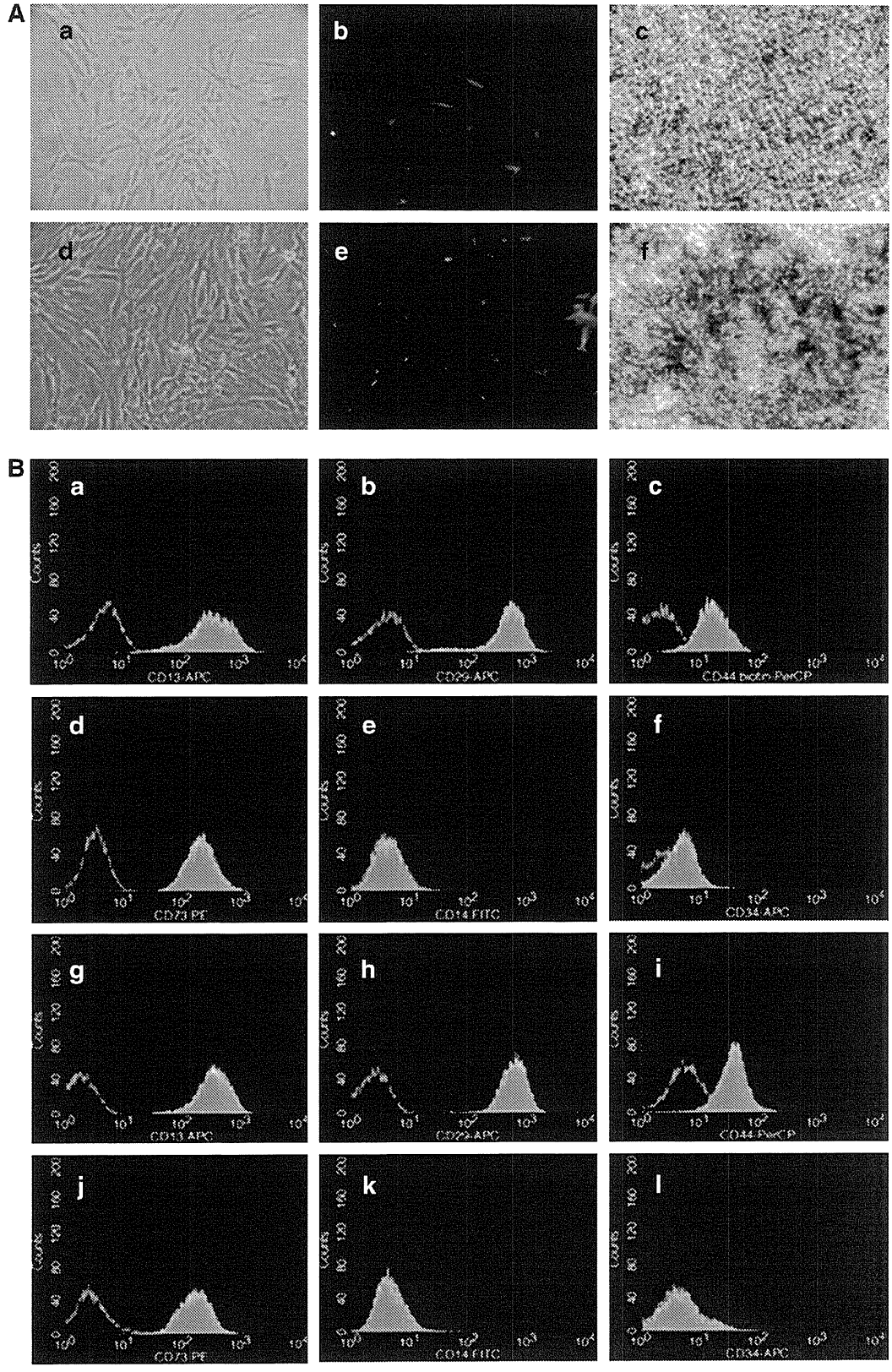

FIG. 1. (**A**) Cell morphology of human dental pulp stem cells (hDPSCs) (**a**) and human deciduous tooth stem cells (hDTSCs) (**d**). Immunofluorescence staining of the stem cell marker STRO-1. hDPSCs (**b**) and hDTSCs (**e**) were positive for STRO-1 (green fluorescence). DAPI was used to observe the nuclei (blue fluorescence). Alizarin red staining: hDPSCs (**c**) and hDTSCs (**f**). (**B**) Typical flow cytometric analysis diagrams for expression of MSC markers CD13, CD29, CD44, and CD73, as well as hematopoietic markers CD14 and CD34 antigens on hDPSCs (**a–f**) and hDTSCs (**g–l**). Unshaded peaks indicated negative control.

Materials Corporation, Osaka, Japan) were implanted into the bone defect that had been made by bone sampling. The dogs were sacrificed 16 weeks after insertion of the dental implant. The mandibles were dissected and cut into smaller blocks. Block sections were fixed in 10% formaldehyde. The sections were embedded in polyester resin (Rigolac, Oken-Shoji, Japan) and polymerized. The specimens were sectioned and ground to about 50 μm thickness using an EXAKT Cutting-Grinding System (BS3000N; EXAKT, Norderstedt, Germany), and stained with toluidine blue. A histological analysis was performed to obtain a general description of the tissue surrounding the implants. The histomorphometrical analysis was done by means of a light microscope (ECLIPSE E-600; Nikon, Tokyo, Japan) connected to a computer (PERFORMANCE JP PIII-700 KER; Gateway, Tokyo, Japan), equipped with a video and image analysis system (Color Chilled 3CCD Camera C-5810; Hamamatsu Photonics K.K., Shizuoka, Japan).

The bone–implant contact (BIC [%] = [total length of bone contact/total length of implant surfaces]×100) was determined as a histomorphometrical parameter.

Statistical analysis

Group means and standard deviations were calculated for each measured parameter. The differences in newly formed bone between the control, PRP, cBMMSCs/PRP, cDPSCs/PRP, and pDTSCs/PRP groups were analyzed using the Tukey–Kramer test following one-way analysis of variance. A p-value of <0.01 indicated statistical significance.

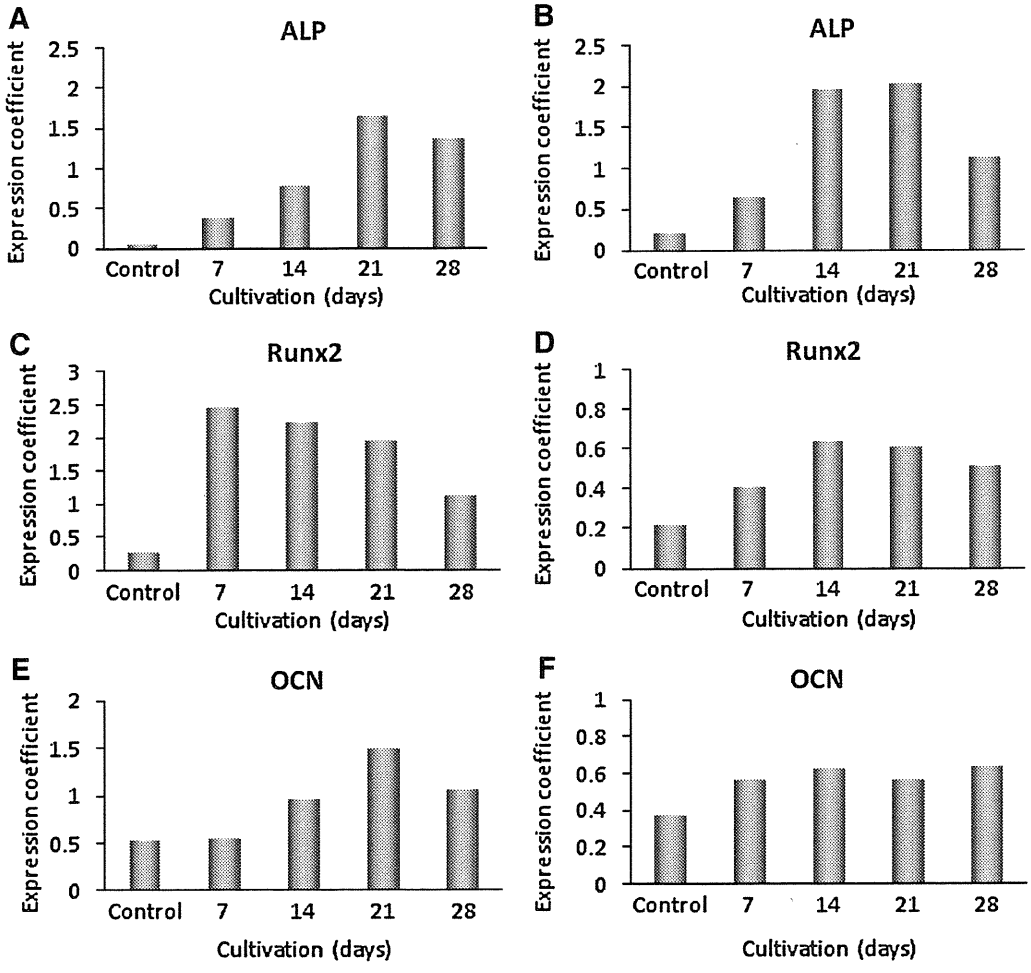

FIG. 2. (**A, B**) Alkaline phosphatase (*ALP*), (**C, D**) *Runx2*, and (**E, F**) *OCN* gene expression levels in hDPSCs (**A, C, E**), and hDTSCs (**B, D, F**) in the conditioning and induction medium. Control cells were cultured in the conditioning medium. On days 7, 14, 21, and 28 of cultivation in the osteoinduction medium, cells were lysed for the extraction of total RNA. Equal amounts of total RNA (50 ng) were analyzed by real-time reverse transcription–polymerase chain reaction, and the relative expression levels of the *ALP*, *Runx2*, *OCN*, and glyceraldehyde OCN, Osteocalcin. 3-phophate dehydrogenase mRNAs in each sample were quantitated by calculating their standard curves as described in the Materials and Methods section. The expression coefficient for each mRNA on the ordinate was calculated by dividing the absolute level of expression of each mRNA (*ALP*, *Runx2*, and *OCN*) with the absolute level of expression of glyceraldehyde 3-phophate dehydrogenase mRNA in each sample in an attempt to compare the levels of gene expression quantitatively among different samples. Each point represents the mean value calculated from five independent replicates, in which the difference was less than 10%. OCN, osteocalcin.

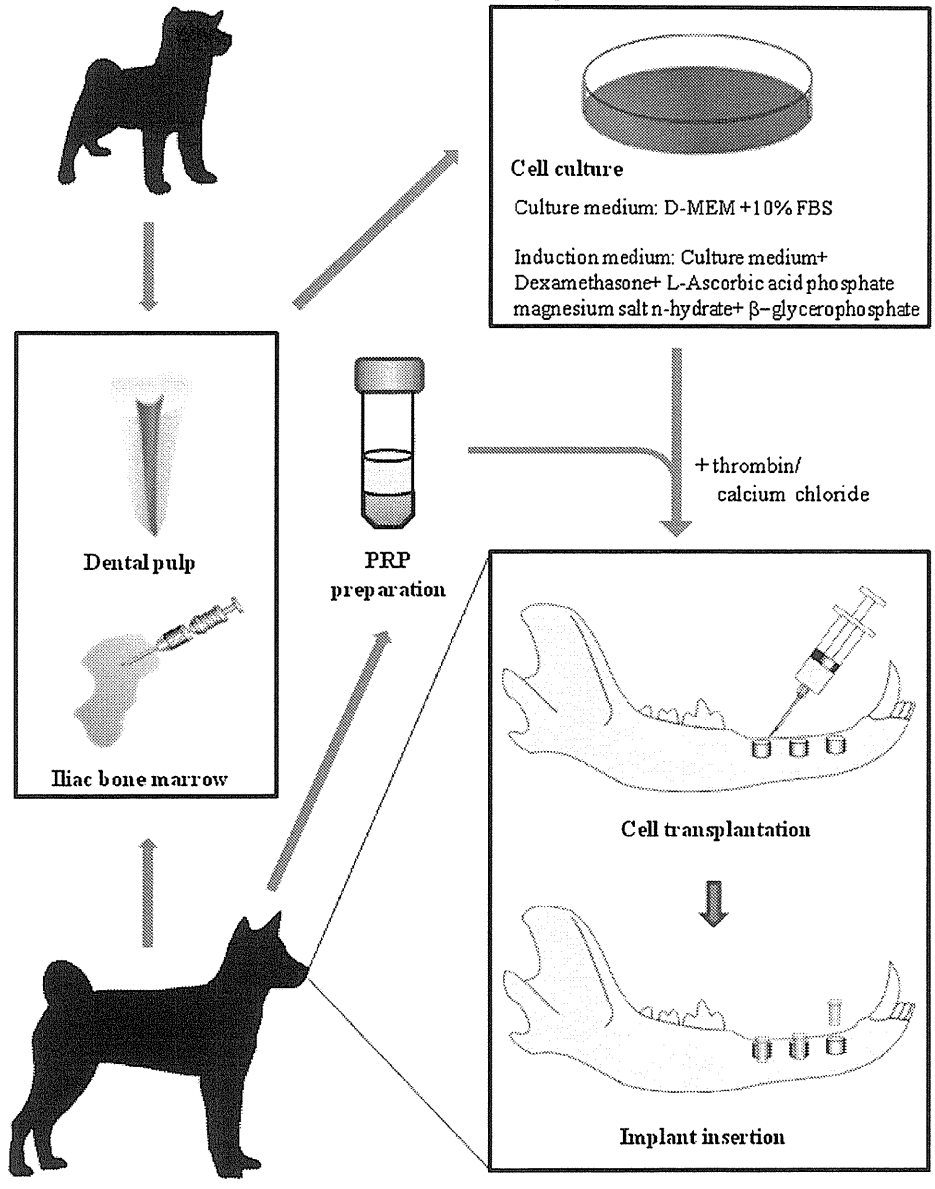

FIG. 3. Schema of the experimental protocol. Hydroxyapatite-coated osseointegrated dental implants were inserted into the bone regeneration areas at 8 weeks after bone injury. PRP, platelet-rich plasma. Color images available online at www.liebertonline.com/ten.

FIG. 4. Histological evaluation of control, platelet-rich plasma (PRP), canine BMMSCs (cBMMSCs)/PRP, canine DPSCs (cDPSCs)/PRP, and puppy DTSCs (pDTSCs)/PRP implants, and the histology of sections around hydroxyapatite-coated dental implants as seen by light microscopy. Sections of representative implants and dental implants are shown from the respective groups. Scale bar = 100 μm (**A, D, G, J, M**); 500 μm (**B, C, E, F, H, I, K, L, N, O**). Hematoxylin and eosin staining was used (**A, D, G, J, M**) with light microscopy, and nondecalcified ground section surfaces were stained with toluidine blue (**B, C, E, F, H, I, K, L, N, O**). (**A**) Section from the control group. (**B**) In the control group, the buccal wall was not sufficiently regenerated for dental implants (lower magnification). (**C**) Control group (higher magnification). (**D**) Section from the PRP group. (**E**) PRP group (lower magnification). (**F**) PRP group (higher magnification). (**G**) Section from the cBMMSCs/PRP group. (**H**) In the cBMMSCs/PRP group (lower magnification), extensive bone–implant contact (BIC) was present. (**I**) cBMMSCs/PRP group (higher magnification). (**J**) Section from the cDPSCs/PRP group. (**K**) In the cDPSCs/PRP group (lower magnification), the fully regenerated buccal bone plate was as wide as the lingual cortex. (**L**) cDPSCs/PRP group (higher magnification). (**M**) Section from the pDTSCs/PRP group. (**N**) pDTSCs/PRP group (lower magnification). (**O**) In the pDTSCs/PRP group (higher magnification), good bone remodeling, as well as extensive BIC, was seen on the sides of the implant.

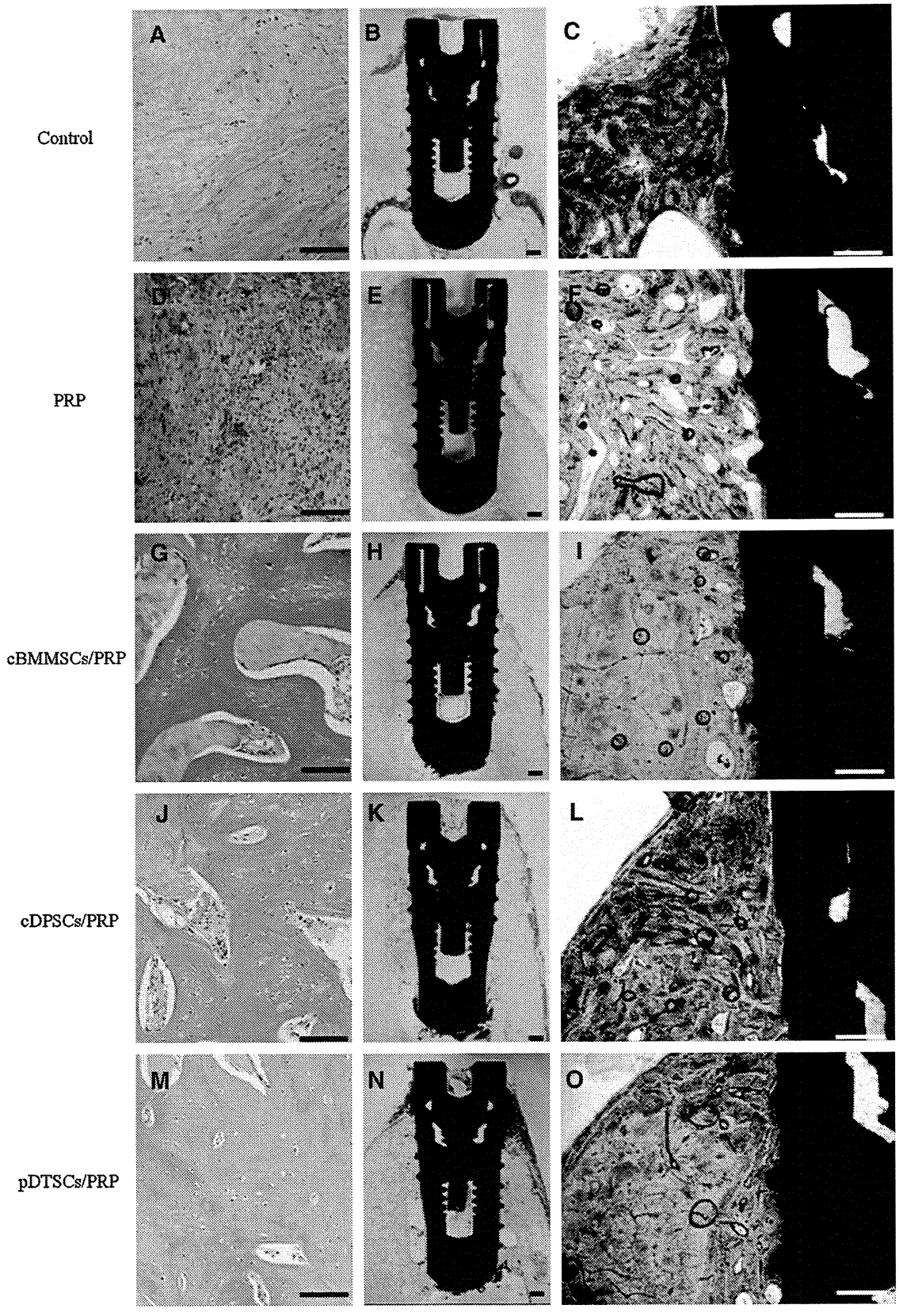
Control
PRP
cBMMSCs/PRP
cDPSCs/PRP
pDTSCs/PRP
A
B
C
D
E
F
G
H
I
J
K
L
M
N
O

Results

Morphological observation and characterization of hDPSCs and hDTSCs

It was confirmed previously that stem cells isolated from the human bone marrow (hBMMSCs) exhibit the characteristics of MSCs. In this study, hDPSCs and hDTSCs displayed a fibroblastic morphology resembling MSCs. Immunofluorescence analysis indicated that hDPSCs and hDTSCs contained STRO-1-positive cells, which is a stem cell marker. In addition, the osteogenic differentiation potential of hDPSCs and hDTSCs was shown by alizarin red staining (Fig. 1A). Moreover, hDPSCs and hDTSCs were negative for hematopoietic lineage markers (CD34) and monocytic markers (CD14). As observed with other BMMSCs, hDPSCs and hDTSCs were mostly positive for CD13, CD29, CD44, and CD73.

Expression levels of ALP, Runx2, *and* OCN *in cultured hDPSCs and hDTSCs in the osteoinduction medium*

Using real-time RT-PCR analysis, the relative amounts of mRNA of the bone-related genes *ALP*, *Runx2*, and *OCN* were measured in hDPSCs and hDTSCs to investigate their osteogenesis potentials. The result showed that the expression levels of *ALP*, *Runx2*, and *OCN* in hDPSCs and hDTSCs in the induction medium increased compared with the levels in the conditioning medium (control), which remained unchanged (Fig. 2A–F).

Comparisons of the expression coefficients on day 21 of cultivation indicated that the relative expression levels of *ALP*, *Runx2*, and *OCN* mRNAs in the induction medium compared with the conditioning medium were 21.9-, 7.2-, and 2.8-fold, respectively, of the values in hDPSCs, and about 10.1-, 4.9-, and 1.5-fold, respectively, of the values in hDTSCs (Fig. 2A–F). Therefore, the expression levels of *ALP*, *Runx2*, and *OCN* mRNAs in hDPSCs and hDTSCs were higher than those at subsequent time points of cultivation by osteoinduction.

In vivo *histological evaluation of implants (cBMMSCs/PRP, cDPSCs/PRP, pDTSCs/PRP, and PRP) compared with the control, and histological findings and histomorphometric analysis around dental implants*

cBMMSCs, cDPSCs, and pDTSCs were trypsinized at day 7 and were used for the implants at a concentration of 1.0×10^7 cells/mL. The cells and PRP were grafted into the defects, HA-coated dental implants were installed, and bone biopsies were performed after 8 weeks (Fig. 3). From the histological observations of the controls and defects filled with PRP, the cortical continuity was never restored, and the cavities were invaded by vascular, fibrous tissue, and few new bone formations (Fig. 4) were seen. On the other hand, cavities filled with cBMMSCs/PRP, cDPSCs/PRP, or pDTSCs/PRP resulted in new bone formation with a tubular pattern along with abundant vascularization at 8 weeks. This pattern reflected normal bone macrostructure with well-differentiated marrow cavity and cortices (Fig. 4). All implants healed uneventfully and remained stable throughout the experimental period. In the control and PRP sites, bone regeneration did not progress sufficiently for dental implantation (Fig. 4A–F). On the other hand, the regenerated bone from cBMMSCs/PRP, cDPSCs/PRP, or pDTSCs/PRP showed newly formed woven and lamellar bone (Fig. 4G–O). Further, the implants exhibited a varying degree of BIC. The BIC was $49.8 \pm 8.8\%$ for the control group, $59.1 \pm 4.3\%$ for the PRP group, $73.6 \pm 6.5\%$ for the cBMMSCs/PRP group, $74.7 \pm 5.8\%$ for the cDPSCs/PRP group, and $76.0 \pm 4.1\%$ for the pDTSCs/PRP group. The BIC of the cBMMSCs/PRP, cDPSCs/PRP, and cDTSCs/PRP groups showed a significant increase in the implant surface compared with the control and PRP, but there were no significant differences among the three cell types (Fig. 5).

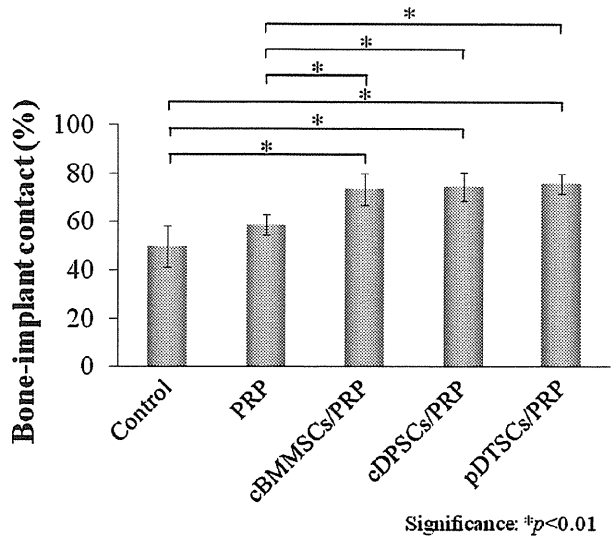

FIG. 5. Histomorphometrical evaluation. Comparison of the mean percentage of BIC (%) among the graft materials. The measurements were made on all threads on both the buccal and lingual aspects of the implants. A statistically significant difference was seen between the cBMMSCs/PRP, cDPSCs/PRP, and pDTSCs/PRP groups and the control and PRP groups. Asterisks indicate significant differences ($^*p < 0.01$).

Discussion

Tissue engineering approaches using stem cells, growth factors, and scaffolds with minimal invasiveness have been attempted for clinical applications and could lead to good clinical results.[11,13] Among these three elements, stem cells are considered to play the most important role. The main cells in stem cells, such as embryonic stem cells (ES cells), induced pluripotent stem cells, and somatic stem cells, should be somatic stem cells, especially MSCs, which have been considered the standard for stem cell sources in TERM. However, with an aging population, it is a weak point in TERM using MSCs that the number, proliferation, and differentiation potential of these cells decline with increasing age. On the other hand, as we grow older, it is easy to suffer the loss of teeth and suffer alveolar bone atrophy; therefore, bone augmentation could be needed for the atrophic area before the placement of osseointegrated implants for the restoration of normal mastication in improving quality of life. This study investigated

the characteristics of allograft DTSCs, compared with autologous DPSCs and BMMSCs, especially by focusing on bone regeneration for dental implants.

At first, it was verified that DPSCs and DTSCs had the characteristics of stem cells (Fig. 1) and bone formation potential (Fig. 2). To confirm these abilities, the differentiation of these cells into osteoblasts was investigated. Osteoblast differentiation, extracellular matrix formation, and subsequent mineralization are needed for bone formation associated with osteogenesis and subsequent osseointegration. It has been reported that dental pulp appears to be an alternative and more readily available source of stem cells. Stem cells from the pulp of permanent teeth (i.e., DPSCs) and from exfoliated deciduous teeth (i.e., DTSCs) have been identified as a novel population of stem cells that have the capacity of self-renewal and multilineage differentiation.[20,22] Moreover, a previous report demonstrated that DPSCs are able to differentiate into an osteoblastic lineage and generate bone,[20,22,25] and human exfoliated deciduous teeth (i.e., SHED: DTSCs) were able to produce woven bone.[25,26] In addition, bone-related genes, such as *Runx2*, also known as transcription factor core binding factor-1, regulate this development and, if disrupted, inhibits bone development.[27] *Runx2* also binds to the OSE2 promoter region of major osteoblast genes, such as *OCN*, bone sialoprotein, osteopontin, and type I collagen, and regulates their expression.[28] It was found that the pattern of *Runx2* and *OCN* gene expression was dependent on the implant surface microtopography.[29] As a direct result of these differences in mineralization and because of the known function of *Runx2* in the regulation of osteoblast differentiation and subsequent mineralization, real-time RT-PCR strategies were used to demonstrate that the expression levels of *ALP*, *OCN*, and *Runx2* genes were enhanced in osteoblasts grown on coated implant surfaces. The results showed that cells differentiating into osteoblasts expressed higher levels of these genes compared with undifferentiated cells cultured in the conditioning medium (Fig. 2). Therefore, DPSCs and DTSCs might have the potential for bone regeneration. In addition, the experimental results *in vivo* showed that the bone defects in the control and PRP alone groups were surrounded by soft tissue that never healed, which were not sufficient for dental implantation. However, the cBMMSCs/PRP, cDPSCs/PRP, and pDTSCs/PRP groups, in spite of the use of an allograft, showed bone regeneration capacity similar to that of BMMSCs with well-formed mature bone and neovascularization (Fig. 4). This response might be dependent on a similar tissue origin embryologically and might show the basic characteristics of MSCs. Moreover, the results showed that no clinical symptoms of pDTSC rejection were observed in the recipient parent dogs and that these dogs did not reject the pediatric DTSCs. It is important to address whether these DTSCs trigger the immunological system of the recipients; therefore, successful bone regeneration and for dental implants with allogenic DTSCs might be related to immunosuppressive activity by stem cells from dental pulp.[17] Further, the values describing the amount of BIC were significantly different between the cBMMSCs/PRP, cDPSCs/PRP, and pDTSCs/PRP groups and the control and PRP alone groups. Berglundh and Lindhe reported a lower BIC for implants placed in a bone-formation-stage approach.[30] After extraction, the defects in the test sites were filled with a demineralized deproteinized bovine bone allograft (DFDBA) material without a barrier membrane. The control sites were not filled, and were left to heal spontaneously with a blood clot, as in the present study. Following the same healing period of 4 months after nonsubmerged implants were placed, the BIC measured along the entire implant surface was 45.8% for the control implants. The BIC percentage was similar to that of the control groups in this study. On the other hand, the cMSCs/PRP, cDPSCs/PRP, and pDTSCs/PRP groups showed a higher percentage in comparison, even after the same healing time. These results might be in good correlation with the present approach with HA-coated implants and bone formation by stem cells, and be due to a bone-promoting effect for these stem cells by PRP, which is known to enhance the formation of new bone and accelerate existing wound healing because it contains an autologous source of platelet-derived growth factors and transforming growth factor-β.[14] In addition to these growth factors, other proteins carried within platelets[31] may act in concert with cytokines released from other cellular sources, thus modulating hemostasis. In short, these results suggest that stem cells, such as cBMMSCs, cDPSCs, and pDTSCs, even if used as an allograft, by reinforcing growth factor concentrations through the application of PRP, lead to improved bone regeneration and osseointegration of dental implants. However, PRP alone was least effective in increasing BIC, and thus PRP in the defect did not result in improved osseous healing.

Taken together, it is important to note that DPSCs and DTSCs have several advantages over BMMSCs derived from other sources; the method for their isolation is not invasive and they can be expanded rapidly *in vitro*.

DPSCs and DTSCs appear to be a potential source of stem cells for bone regeneration in dental implants as an alternative to BMMSCs, and DTSCs do not stimulate allogeneic graft rejection by the recipient organism. These results, concerning DTSCs especially, might indicate an important and promising approach in terms of allogeneic stem-cell bone therapy as part of the stem-cell banking system.

Acknowledgments

The authors wish to thank Drs. Wataru Katagiri, Kazuto Okabe, Tomoyuki Kohgo, Yudai Nishino, Masato Fujio, and the members of the Department of Oral and Maxillofacial Surgery and Ms. Matsuba Kazuko of the Laboratory of Medicine, Nagoya University, Graduate School of Medicine for their help, encouragement, and contribution to the completion of this study. This work was partly supported by Fumiaki Miyaji, Yusuke Yoshihara, and Yumiko Nakao of the Japan Medical Materials Corporation and Grants-in-Aid for Scientific Research (No. 20659297, 21390507, and 21791848) from the Japan Society for the Promotion of Science and Akasaki Memorial Research Project by Nagoya University.

Disclosure Statement

No competing financial interests exist.

References

1. Branemark, P.I. Osseointegration and its experimental background. J Prosthet Dent **50,** 399, 1983.
2. Wen, X., Wang, X., and Zhang, N. Microrough surface of metallic biomaterials: a literature review. Biomed Mater Eng **6,** 173, 1996.